Simulations of the North American Monsoon System. Part I: Model Analysis of the 1993 Monsoon Season

STEPHEN M. SALEEBY AND WILLIAM R. COTTON

Colorado State University, Fort Collins, Colorado

(Manuscript received 3 March 2003, in final form 18 November 2003)

ABSTRACT

The North American monsoon system is known to produce significant summertime precipitation on the west coast of Mexico and the southwestern United States, with some areas receiving greater than 50% of their yearly rainfall between the months of July and September. The onset of the monsoon is attributed to a shift in the large-scale upper-level anticyclonic flow over the central United States, and the associated increases in moisture flux and resulting precipitation are tied to the low-level jets from the Gulf of California and the Gulf of Mexico. Individual monsoon surge events vary in intensity, as does the magnitude of the diurnal cycle of the low-level jets and precipitation. Numerical modeling and forecasting of these interacting large- and mesoscale monsoon features is often difficult in terms of accurately recreating the varying flow regimes aloft and near the surface and over both the flat and steep terrain that are encompassed within the monsoon region of influence.

The Regional Atmospheric Modeling System (RAMS) at Colorado State University has been utilized to investigate seasonal monsoon simulations for the 1988 (United States drought), 1993 (Midwest flood), and 1997 (El Niño year) monsoon seasons. In Part I of this paper the credibility of RAMS, as far as its ability to reproduce observed features of the North American monsoon system, is evaluated. Part II provides interseasonal comparisons of model-simulated monsoon features from the three simulated extreme seasons and results of sensitivity studies to SSTs and soil moisture variability. Part III presents the development of potential vorticity anomalies associated with convection over Mexico and their downstream influence over the central United States.

1. Introduction

The North American monsoon is recognized as a seasonally varying phenomenon resulting in a large-scale reversal in the precipitation pattern over the United States and Mexico. Low-level moisture surges along the western coast of Mexico and the Gulf of California (GoC) occur periodically throughout the monsoon season and are followed by an increase in the amount of rainfall over northwest Mexico and the southwest United States. Northern Mexico and southern Arizona often acquire over 60% (Douglas et al. 1993) and 40% (Jurwitz 1953; Bryson and Hare 1974), respectively, of their yearly rainfall from surge events during June–September. Moisture surges from the GoC are known as the northernmost extension of the Mexican monsoon (Douglas et al. 1993; Stensrud et al. 1995), and they vary from year to year in duration, intensity, and in the extent of their northward push (Brenner 1974). As surges make their northward progression up the GoC, they are known to influence the surface by reducing the temperature and by increasing the mixing ratio, sea level pressure, and southerly winds (Hales 1972; Brenner 1974; Douglas 1995). Following monsoon onset the low-level reversal in the winds from northwesterly to southerly plays a key role in the transport of low-level moisture northward along the GoC and into the United States (Sadler et al. 1987; Badan-Dangon et al. 1991). Only recently, with better observations and modeling studies, has the prominence of a low-level jet (LLJ) within the GoC been recognized as a primary mechanism for transporting low-level moisture into Arizona and New Mexico (Douglas 1995; Stensrud et al. 1995, 1997). Monsoon onset and the type of monsoon season (wet or dry) is largely controlled by the position of the U.S. high pressure ridge, with a northwest (southwest) shift in the anticyclone correlating with wet (dry) monsoon years (e.g., Carleton et al. 1990; Higgins et al. 1998). The development of individual surges and their strength is closely tied to the interaction of midlatitude troughs and the passage of tropical easterly waves (Stensrud et al. 1997). It is suggested that the development of the strongest surges occurs if a midlatitude trough passes the western United States a few days prior to the passage of an easterly wave. In contrast, the simultaneous interaction of these two systems suppresses surge advancement into the southwest United States (Stensrud et al. 1997).

The Regional Atmospheric Modeling System

Corresponding author address: Stephen M. Saleeby, Atmospheric Science Dept., Colorado State University, Fort Collins, CO 80523.
E-mail: smsaleeb@atmos.colostate.edu

(RAMS) at Colorado State University (CSU) has been used in this current study to simulate the 1988, 1993, and 1997 monsoon seasons. The 1993 season will be the focus of this paper. The primary purpose of this investigation is to compare model realizations to the observed features of monsoon circulations from the large scale to mesoscale and to gain a better understanding of the linkage between the monsoon and precipitation that occurs on the downstream subsiding branch of the large-scale anticyclonic circulation over the central United States. Part I of this three-part paper examines the abilities and limitations of the model in capturing the characteristics of the monsoon with emphasis upon the large-scale circulation, vertical and horizontal extent of moisture surges, and the relative influence of the GoC LLJ and Gulf of Mexico (GoM) LLJ. Diurnal variations in convection, precipitation, and the GoC LLJ will also be presented, as well as the modeled quantitative precipitation forecasts (QPFs) from use of both the Kuo and Kain–Fritsch cumulus parameterizations. Results are compared with the National Centers for Environmental Prediction–National Center for Atmospheric Research (NCEP–NCAR) reanalysis, surface observations, rain gauge precipitation data in the United States and Mexico, and the established conceptual models of monsoon characteristics. Part II will provide interseasonal comparisons of model simulations of the 1988, 1993, and 1997 seasons and results of sensitivity studies to SSTs and soil moisture variability. Part III will address potential vorticity anomalies associated with convection over Mexico.

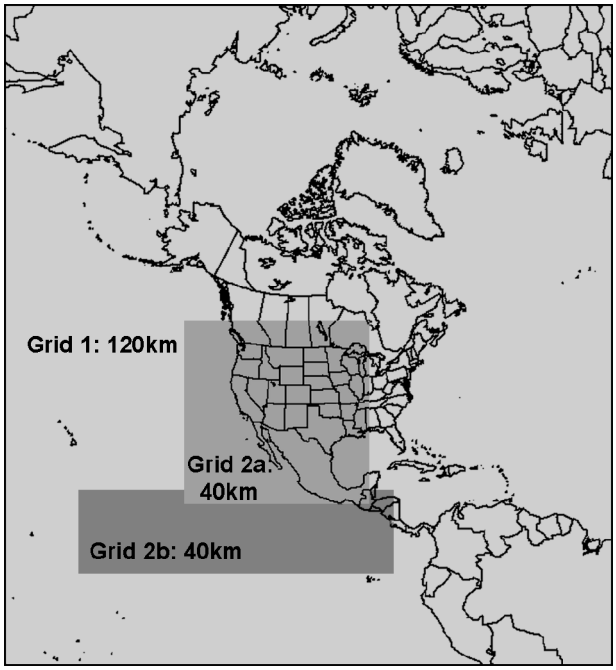

FIG. 1. RAMS model three-grid configuration used in seasonal simulations of the North American monsoon. Unless otherwise noted, all figures depict model analyses produced from grid 2a for the 1993 seasonal simulations. The figure border shown is the border for grid 1.

2. Model description

The seasonal monsoon simulations were run with the nonhydrostatic version of the RAMS model on an Arakawa C grid with sigma-*z* terrain following coordinates (version 4.3) (Cotton et al. 2003). The model is arranged with a three-grid configuration (Fig. 1) whose outermost grid (115 × 90 × 36 grid points) has a resolution of 120 km and covers much of the northwest hemisphere with the center of the domain over the southwest United States. There are also two nested grids, using two-way nested feedback, with 40-km spacing: one covers Mexico and the western two-thirds of the United States (104 × 110 × 36) and the other covers the eastern Pacific ITCZ (188 × 59 × 36). The outermost grid is allowed to consume such a large region so as to include the impact of the large-scale circulations. The U.S.–Mexico grid is the focus region for the monsoonal flow from Mexico that subsequently influences the Great Plains region. The ITCZ grid is included to better resolve the circulation from the warm tropical Pacific and its influence on monsoon surge events. The model extends vertically into the stratosphere with a vertically stretched grid whose maximum spacing is 1000 m at the highest model level; this allows for higher resolution in the boundary layer where conditions vary most rapidly with height. The model is run with single-moment liquid and ice phase bulk microphysics (Walko et al. 1995), two-stream Harrington radiation (Harrington 1997; Harrington et al. 1999), Land Ecosystem Atmosphere Feedback (LEAF-2) land surface model (Walko et al. 2000), Kuo (Kuo 1965, 1974) and/or Kain–Fritsch (Kain and Fritsch 1990, 1992, 1993) convection parameterization, Smagorinsky horizontal diffusion (Smagorinsky 1963), vertically parameterized diffusion of Mellor and Yamada (1974), and Klemp–Wilhelmson lateral boundary conditions (Klemp and Wilhelmson 1978). At the time when the initial simulations were performed, the Kuo convection scheme was the only convection parameterization available in the RAMS model, and thus results are presented from those simulations. Recently, the Kain–Fritsch scheme has been added as a model option (Castro et al. 2002), and brief results are presented from preliminary testing.

Model initial conditions were assimilated with NCEP–NCAR reanalysis data, surface observations, rawinsonde upper-air datasets, weekly averaged Reynolds sea surface temperatures (Reynolds and Smith 1994) (see Fig. 2), Food and Agriculture Organization of the United Nations (FAO) variable soil type, standard RAMS Olson Global Ecosystem (OGE) vegetation datasets, and heterogeneous soil moisture. The sea surface temperatures in the model are updated throughout the duration of the simulations via a time-weighted interpolation of the weekly averaged SSTs; thus, the model is able to run continuously in a synoptic mode for the

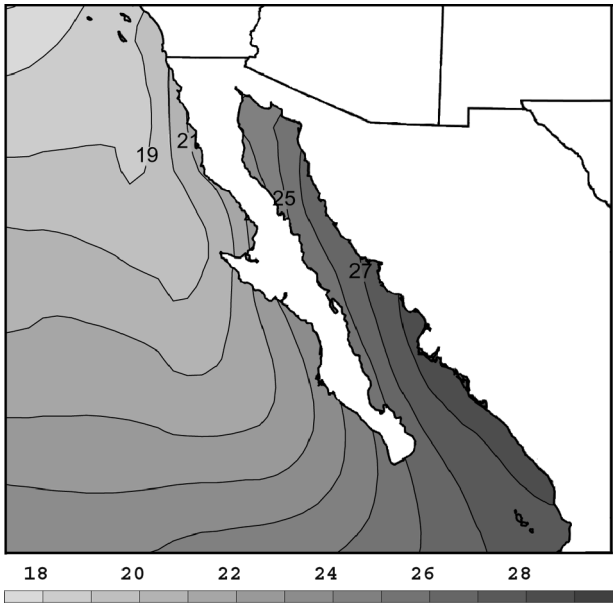

FIG. 2. Weekly averaged SST field (°C) for the week of 4 Jul 1993, mapped to the RAMS model grid from the Reynolds weekly averaged SST files.

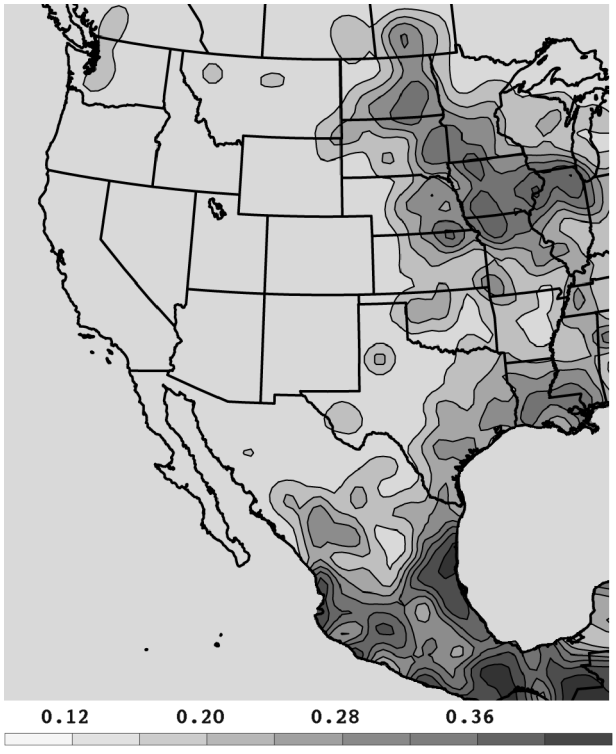

FIG. 3. Volumetric soil moisture estimated for 4 Jul 1993 from the API technique, based upon a weighting function of the daily accumulated precipitation from the previous 90 days. The U.S. daily precipitation was obtained from the hourly rain gauge network, and Mexican precipitation was made available from the Mexican daily rain gauge reports. A value of 0.42 equals 100% saturation.

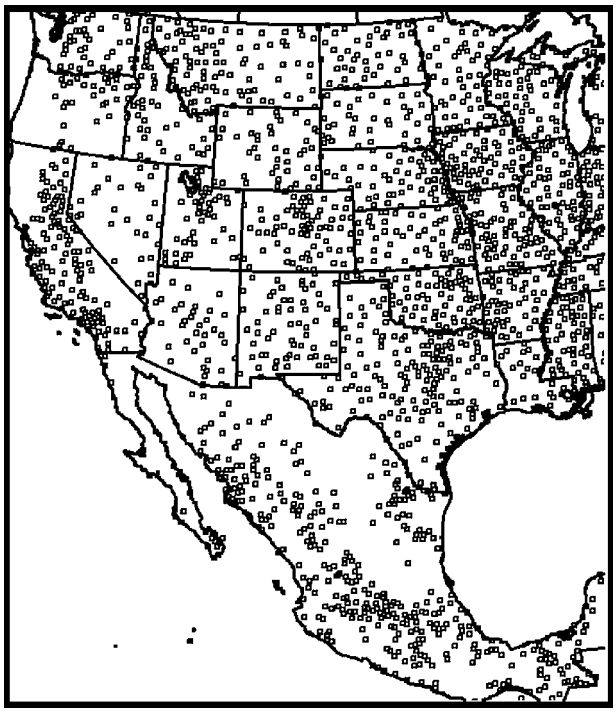

FIG. 4. Rain gauge data points used in API volumetric soil moisture estimations and in plots of the accumulated seasonal precipitation. Plot depiction has undergone station declustering in regions where a large number of gauges are present within a small location. The station spacing following declustering retains a maximum resolution of 20 km.

duration of the monsoon period. The soil moisture was estimated using the Antecedent Precipitation index (API) method, which provides an estimate via a weighting function that considers the previous 90 days of daily recorded observed precipitation (Blanchard et al. 1981). This method was chosen over other soil moisture products because of the ability to estimate soil moisture over Mexico from a network of daily precipitation gauge data (see Figs. 3 and 4). Also, many other soil moisture products do not provide data back to 1993 and do not cover areas other than the continental United States. Precipitation data for the API estimation comes from the U.S. hourly rain gauge network and the Mexican daily rain gauge data. (Data from Mexico was provided by A. Douglas 2001, personal communication.)

For the duration of the simulations, NCEP–NCAR reanalysis data are assimilated at 6-h intervals for use as nudging files. The lateral boundaries are nudged on the five outermost grid point on a 15-min time scale on the 120-km parent grid. Very light internal gridpoint nudging is also performed on the 120-km parent grid on a 2-day time scale. Castro and Pielke 2004, manuscript submitted to *J. Geophys. Res.*) found that without light interior nudging, the nonclimate version of RAMS, used here, begins to incur a logarithmically increasing difference in time between the model *initialized* kinetic energy and the model *realized* kinetic

energy. They found this error to increase as the domain grid spacing or domain size is increased. The light internal nudging prevents the model large-scale fields from severely drifting from reality over time, while allowing the model to develop the mesoscale features crucial to the monsoon circulation and influences over Mexico and the United States. Our own test simulations have shown that without internal nudging, the model large-scale height field begins to significantly deviate from reality after seven model days; as a result, surface precipitation fields and monsoon surges are very missimulated. At this point, the benefits of light internal nudging on the coarsest grid outweigh the slight influence that it may impose upon the finer scale grids. In the future, improved techniques to alleviate this problem will be implemented.

Model control simulations were run for the 1988 U.S. drought year (wet monsoon year) (onset 24 June), the 1993 U.S. flood year (dry monsoon year) (onset 3 August), and the 1997 El Niño year (onset 21 July). The onset dates and monsoon type for the 1988 and 1993 seasons were obtained from the precipitation index method and climatology, respectively, from Higgins et al. (1997), and the 1997 onset date was determined as the first day of the first seasonal monsoon surge that pushed unusually high moisture air across the U.S.–Mexico border into Arizona and west New Mexico. Designated onset dates are also marked as the first sudden onset of warm season precipitation over southern Arizona and/or New Mexico. Both rain gauge data and modeled precipitation agree with the onset day of precipitation just north of the U.S.–Mexico border over the desert southwest. The control runs for 1993 and 1997 cover the period from 1 July to 31 August and the 1988 season was run from 1 June to 15 August.

3. RAMS model monsoon characteristics

a. Summary of modeled surge events

The 1993 monsoon season began with its first seasonal surge event into Arizona on 3 August. This is a fairly late start to the monsoon, when the average onset date in the United States for the period from 1963 to 1994 is 7 July (Higgins et al. 1997, 1998). Studies suggest that late (early) monsoon starts, typical of dry (wet) monsoon seasons, are preceded by wet (dry) winters (Higgins et al. 1998). The RAMS model denotes three distinct surge events between 3 and 31 August, whereby a moisture surge is denoted as a distinctive northward progression of the monsoon moisture boundary from near the Arizona–Mexico border into central Arizona. The first surge is from 3 to 10 August with the peak in the northward translation occurring 6 August in the model. The second is from 9 to 23 August with a peak on 21 August. There is a lull in mixing ratio advancement on 24–25 August but not a full recovery before the next strong surge from 26 August through the end of the month, with a peak near 29 August. Periods between modeled surge events are characterized by diminished flow from the GoC, westerlies and lowered mixing ratios over the southwest, return migration of the mid- to upper-level anticyclone, and propagation of short waves to the north of the monsoon ridge [consistent with Adang and Gall (1989)].

Daily averaged time series plots of surface dewpoint, temperature, and meridional wind from surface observations at Yuma, Tucson, and Luke Air Force Base in Arizona are compared, in Fig. 5, to the relative nearest model grid points at the lowest model level (72 m AGL) for the identified surge periods. (The model data were also interpolated to the surface, but results did not reveal any improvement or better representation of the surface station conditions, and thus the lowest model level data are presented.) Fuller and Stensrud (2000) identify surges from surface observations by a rapid increase in dewpoint, decrease in temperature, wind shift to southerly flow, and a wind speed increase. They require the Yuma dewpoints to reach and maintain 15.6°C and the southerly winds to exceed 4 m s^{-1} at a single reporting time. Each of the surge periods mentioned above fulfills the dewpoint and temperature criteria at each station and model closest grid point (despite being daily averaged quantities); each surge period also reveals an increase in the meridional wind with a shift to southerly flow at the start of the surge periods. The model simulates best the station dewpoints and temperature; it deviates more significantly in reproducing the meridional wind, though the general trends during surge and nonsurge periods are captured and southerly winds exceed the minimum requirement for at least one reporting time. The most noticeable discrepancy between the observations and model time series is the timing of surge onset. There is a slight time delay in the model onset for each surge event though, once the surge reaches the observations points (closest model grid points), the dewpoint increases rapidly and remains elevated throughout the surge. As will be shown in section 3c, the model tends to underpredict the northward propagation speeds of most surges. This delays surge onset into the United States, but it does not prevent the surges from occurring in the model and does not limit the dewpoints from reaching similar maxima to those seen the in the observations. Lastly, the short duration surge centered around 14 August, apparent from the dewpoint time series, appears to be relatively weak compared to the other observed surges in the observations and model simulation and, therefore, does not meet the dewpoint magnitude criterion.

b. Upper-level analysis and vertical motion

In its early stages in the model, the monsoon begins as an increase in daily convection and precipitation in southern Mexico; as the season progresses, the onset of daily convection begins to push farther up the western

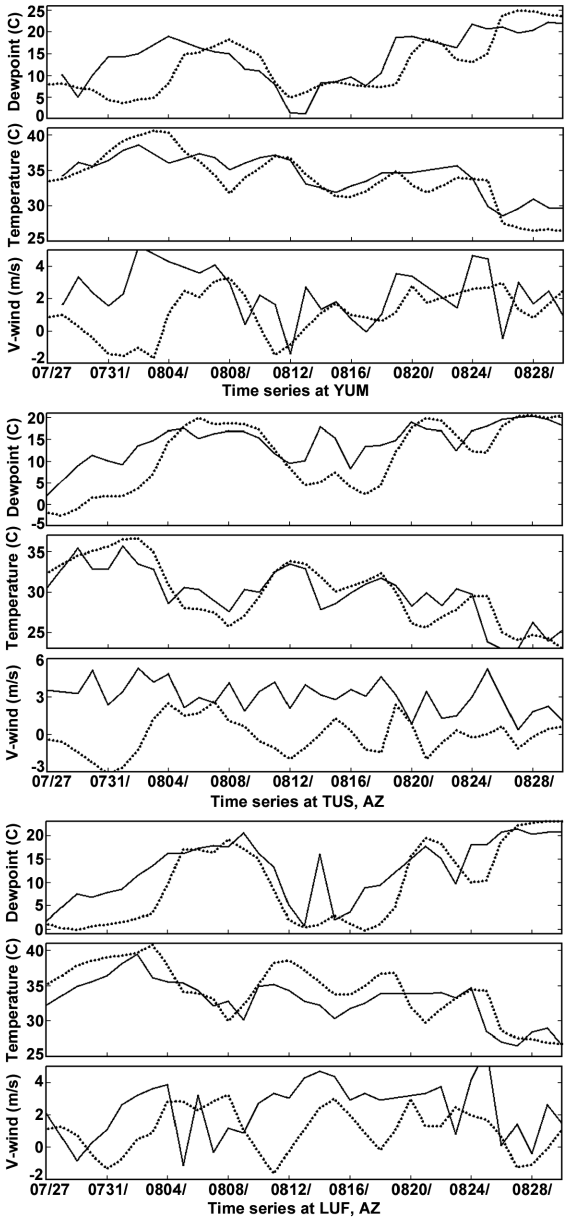

FIG. 5. Daily averaged time series of dewpoint, temperature, and meridional wind component at Yuma (YUM), Tucson (TUC), and Luke AFB near Phoenix (LUF) from the observations (solid) and model closest grid point (dotted). The 0000, 0600, 1200, and 1800 UTC values were averaged to get the daily averaged value since the diurnal variation is often greater than the change seen between surge and nonsurge periods. This effectively declutters the time series and removes the diurnal variability.

slopes of the Sierra Madre range (Douglas et al. 1993; Stensrud et al. 1995). This slow push of convection and the moisture boundary is typically contained south and east of northwest Mexico until the first significant westward or northward shift in the mid- to upper-level North American high pressure ridge (e.g., Bryson and Lowry 1955; Adang and Gall 1989; Carleton 1987). This initial shift in the large-scale anticyclone precedes the first surge of moisture into the United States by approximately 3–5 days in the model. The delay between the beginning of the westward movement and the start of the monsoon burst is evident for each surge event during the 1993 season, and the distance and time duration of the shift varies between surge events. At its maximum east–west extent for the 1993 surges, the anticyclone shifts from central Louisiana into central Arizona.

The 500-mb streamlines averaged over a period of 28 days before and after onset (Fig. 6) reveal a slight seasonal westward shift in the monsoon high; this variation appears small due to the seasonal averaging, which includes both surge and nonsurge periods. Figures 7a and 7b show the same monsoon high but averaged for 7 days before and after the onset surge event, and Figs. 7c and 7d display the same surge averages produced from the NCEP–NCAR reanalysis data. The large-scale anticyclone undergoes a significant displacement to the west-southwest and exhibits a distinct flattening of the ridge to the north with predominantly zonal flow along its northern edge; these characteristics agree with the known patterns exhibited during a dry monsoon (Carleton 1987; Carleton et al. 1990; Higgins et al. 1998). Despite significant resolution differences between the model and the NCEP–NCAR reanalysis, they compare quite well with respect to the location of the rotation center of the large-scale anticyclone. The light internal grid nudging with the NCEP–NCAR reanalysis allows the model to closely retain the observed large-scale features over time while still resolving the monsoon mesoscale features (to be shown). In the 7-day period before and after the surge onset, southerly flow into western Arizona at mid levels is present; the primary difference after onset is the increased magnitude of the low- and midlevel flow over the GoC and southwest United States coincident with the westward translation of the anticyclone. The positioning of the 500-mb ridge is also coincident with the development of anticyclonic flow near the surface in western Arizona and northern Mexico.

During the transition to monsoonal flow, the vertical velocity field responds to the shift in the position of the anticyclone. Compared to wet monsoon years, a typical dry monsoon is characterized by strong southwesterly flow and enhanced rising motion and precipitation over the Great Plains and Midwest (Higgins et al. 1998). From Fig. 6 this southwesterly flow over the Great Plains is quite evident from the monthly average, though the single-surge average from Fig. 7 reveals a pattern more indicative of the climatological mean from Higgins et al. (1998); while the seasonal average tends to support the 1993 as a dry monsoon, there are significant episodes of strong monsoonal flow over the Southwest that also influence the central plains. Following the 1993 onset, the vertical velocity at 300 mb increases primarily along the Sierra Madre Occidental (SMO), Arizona, New Mexico, Utah, and Colorado (Fig. 8a). There is also a region of large-scale subsidence at 300 mb over

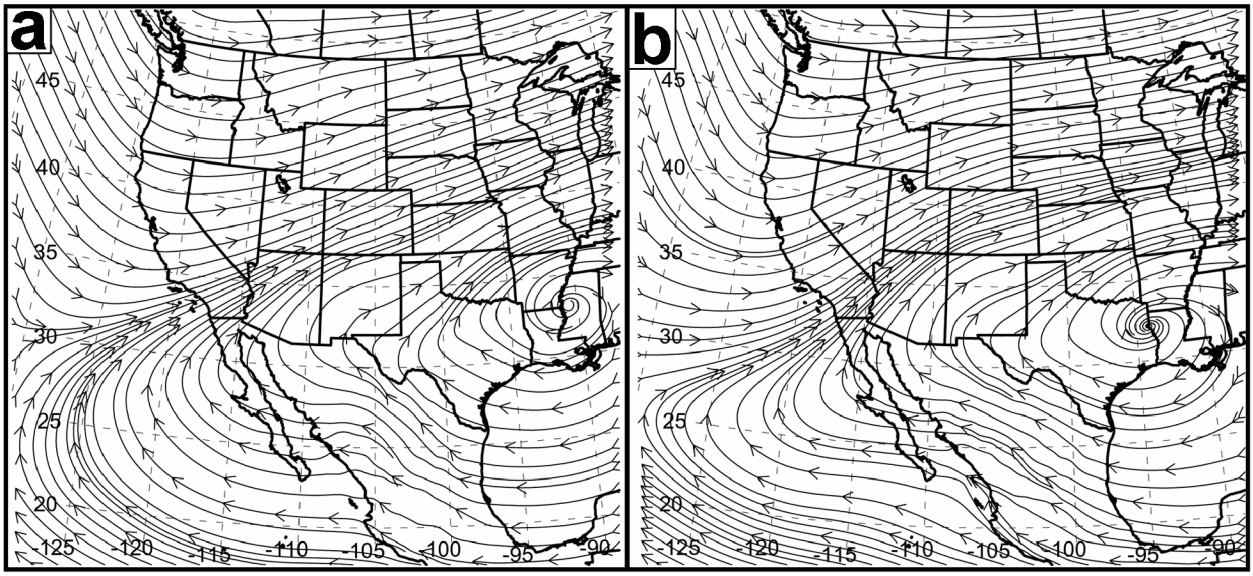

FIG. 6. Model 500-mb streamlines averaged (a) before and (b) after onset. Fields are averaged for the 28-day period pre- and postmonsoon onset. The large-scale anticyclone begins to transition approximately 3–5 days prior to onset.

the Great Plains and part of the Midwest. The 300-mb divergence difference field offers another perspective into the vertical velocity and the potential for the vertical transport of moisture (Fig. 9); the divergence features in this plot are quite comparable to the field derived from the NCEP–NCAR reanalysis. Despite the resolution differences between RAMS and the NCEP–NCAR reanalysis, both divergence difference fields indicate upper-tropospheric divergence (upward motion) following onset over the monsoon region and U.S. Southwest and upper-tropospheric convergence (subsidence) over much of the Midwest and Great Plains. The out-of-phase relationship in the vertical motion field between the Southwest and the Great Plains agrees with previous observational studies (Higgins et al. 1997, 1998), though this relationship is not discernable in every season (Cavazos et al. 2002).

The changing pattern in the upper-level vertical motion primarily takes on a westward shift after monsoon onset, which corresponds to the shift in the upper-level horizontal winds. Regions of postonset descending motion, which were originally along the western or northern extent of the ridge, find themselves positioned along the subsiding branch of the monsoon ridge and to the backside of the anticyclone. The resulting pattern of the average precipitation rate difference mimics the patterns of the vertical velocity and divergence fields over the SMO, Arizona, and New Mexico (Fig. 8b) [also shown in Higgins et al. (1998)]. The model is consistent with previous works, such that it indicates an increase in precipitation over the Southwest and a decrease over portions of the Great Plains and Midwest (e.g., Douglas et al. 1993; Mo et al. 1997). Over the Great Plains and lower Midwest, though, there are subregional areas that exhibit an increase in precipitation despite subsidence being the dominant pattern. This suggests that perhaps the uplift associated with the Great Plains LLJ does little to influence the 300-mb vertical velocity field or that precipitation systems develop upstream from the plains and are a source of precipitation for the Great Plains during the monsoon season.

c. Moisture sources at low and midlevels

Typical surge events are marked by a definitive northward progressing plume of low-level moisture from the GoC and SMO that tends to mainly influence the southern half of Arizona and New Mexico for periods of a few days up to about a week (e.g., Hales 1972; Adang and Gall 1989; Stensrud et al. 1997). Figure 10 displays the low-level mixing ratio and streamline fields for the 28- and 7-day averages before and after monsoon onset, respectively. Of the model levels within 1 km of the surface near the northern GoC, the 233-m level represents the greatest relative magnitude for both moisture and winds. Both the short- and long-term averages reveal a significant shift in the winds at the 233-m model height from westerly to southerly along the GoC during the transition to a burst phase. Corresponding to this is an increase in the mixing ratio in southern Arizona from 6 to 12 g kg^{-1} for the monthly average, which incorporates several surge and retreat cycles. The individual onset surge average shows an even greater increase from 4 to 14 g kg^{-1}. A case study by Adang and Gall (1989) also reveals similar jumps in near-surface mixing ratio in southern Arizona from ~4 to 12 g kg^{-1} with passage of the moisture boundary, followed by a drying phase as the burst phase subsides.

Several cross sections taken along the length of the initial surge event reveal the northward progression and

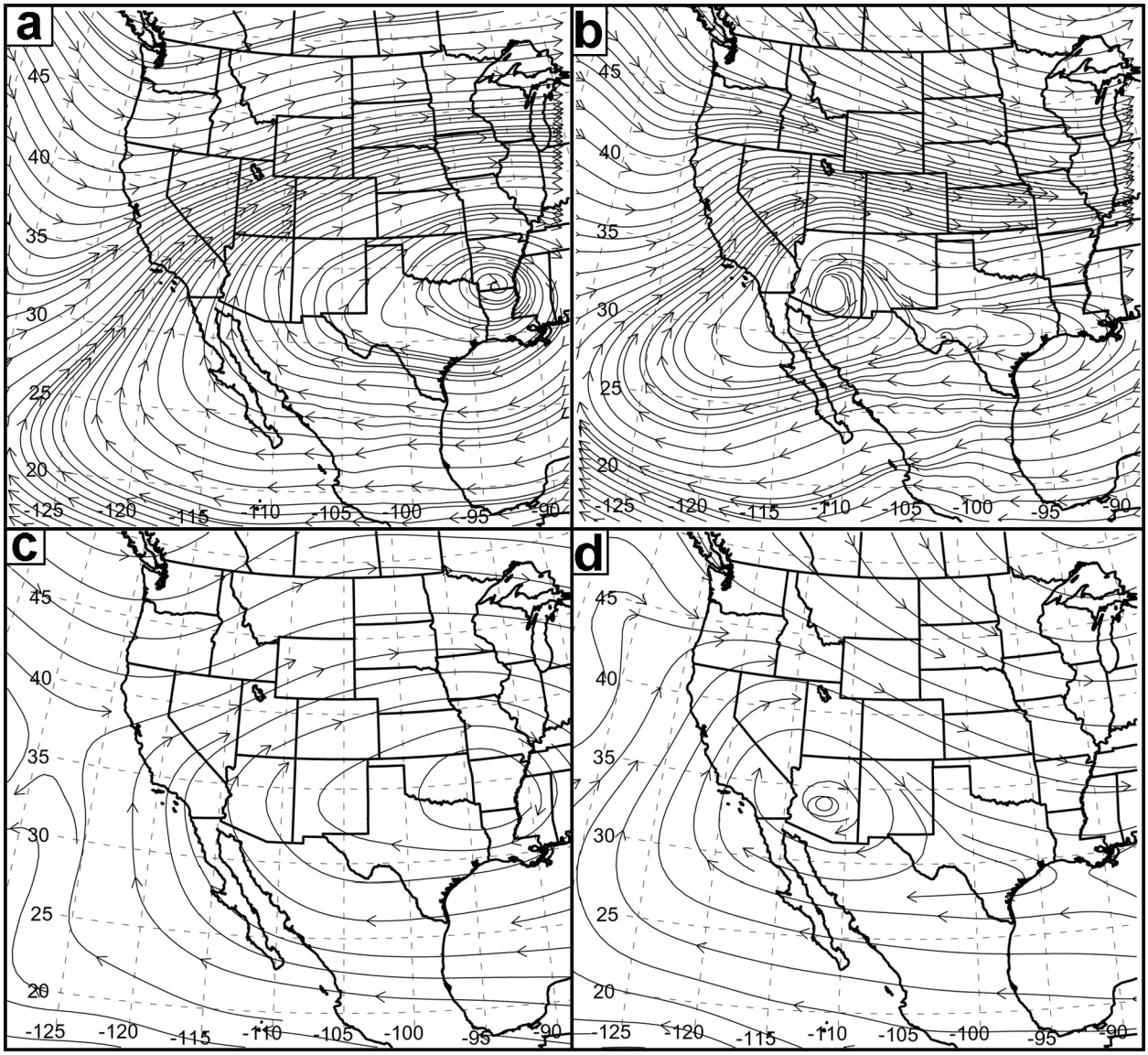

FIG. 7. The 500-mb streamlines averaged (a), (c) before and (b), (d) after onset from the (a), (b) RAMS analysis and (c), (d) NCEP–NCAR reanalysis. Fields are averaged for the 7-day period pre- and postmonsoon onset.

evolution of the surge over time. Figure 11 displays the location of the cross section and the vertical structure of the surge at 2-day intervals from 29 July to 6 August 1993. As it propagates northward, the surge ushers in cooler temperatures and very moist air from the southern GoC and maintains strong horizontal and vertical moisture gradients (up to 500 m in the vertical). Over time the advection of cooler air toward the northern GoC coast also results in a strengthened temperature gradient along the front edge of the surge. As the surge develops, the near-surface winds behind the leading edge increase in the direction of surge motion; this results in stronger vertical motion along the northern moisture boundary due to increased surface convergence with the prevailing northerly flow downstream. As the surge encounters increased surface friction over land, it resembles a density current or undular bore in that it develops a distinct ''nose'' along the leading edge of the mixing ratio contours whose vertical depth is greater than that to the rear of the initial boundary. The surge differs from a density current, though, in that it is limited in its northward progression, is controlled by the strength of the low-level flow from the GoC, and experiences a retreat phase following its northernmost progression. The propagation speed for this particular modeled surge event is rather slow at approximately 2 m s^{-1}. Other modeled surge episodes reveal propagation speeds reaching from 5 to 6 m s^{-1}, which is still 2 to 3 times slower than several of the modeled surges presented by Stensrud et al. (1997). Though the surge velocity is slower than

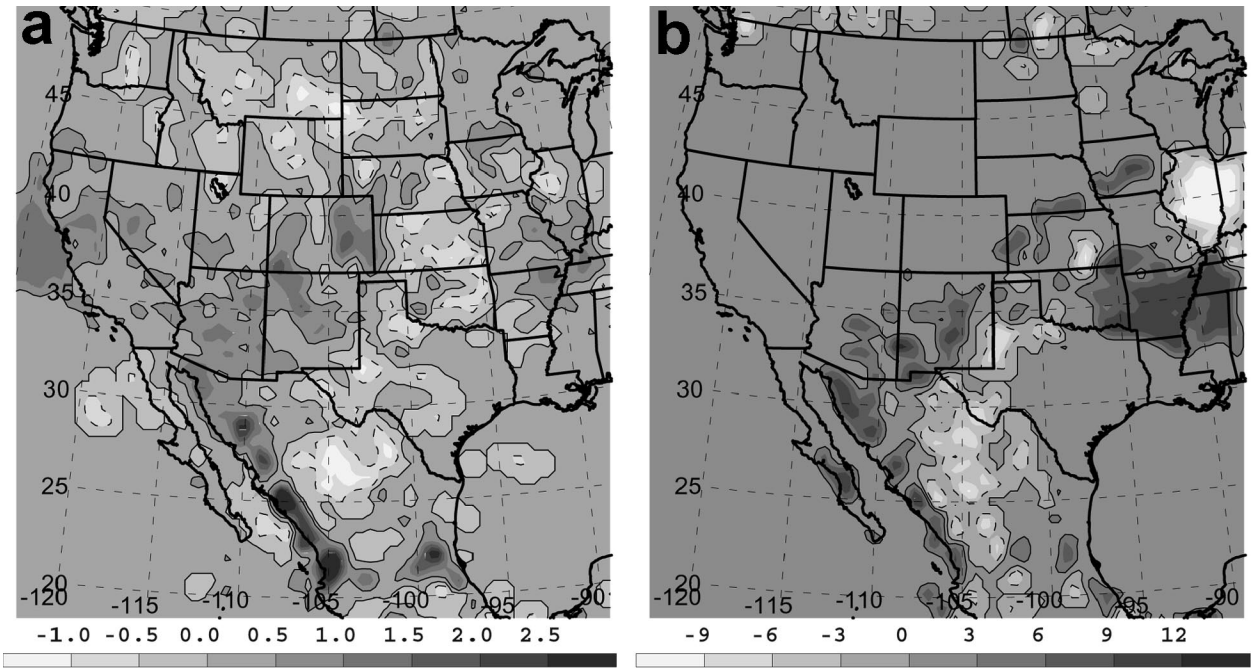

FIG. 8. Model 300-mb (left) vertical velocity difference (cm s^{-1}) and (right) precipitation rate difference (10^3 h^{-1}) between the 28-day pre- and postonset averages. Positive values (darker shading) indicate an increase following monsoon onset. Solid (dashed) contours surround positive (negative) values.

anticipated, the low-level moisture, temperature, and wind fields tend to agree with the characteristics of surge events.

Plots of the average moisture transport magnitude at 233 m above the surface provide insight into both the presence of excess moisture and the strength of the transport mechanism that drives the moisture into the U.S. Southwest (Fig. 12). The monthly average shows

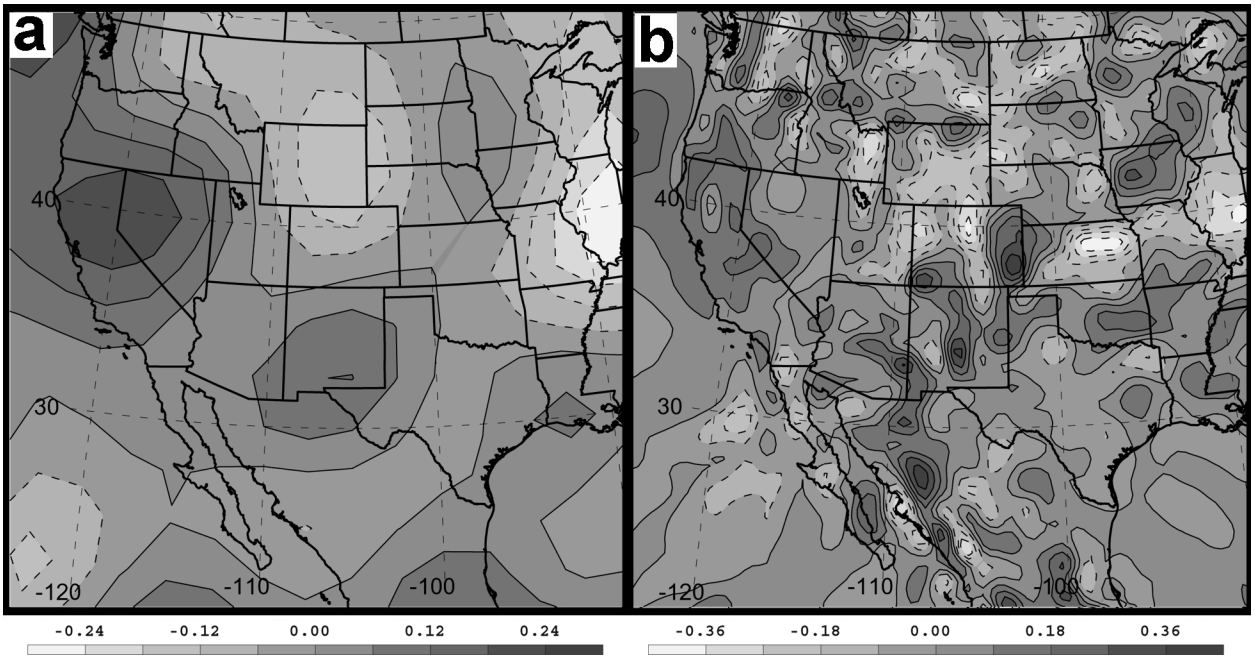

FIG. 9. The 300-mb horizontal divergence difference (10^5 s^{-1}) between the 28-day pre- and postonset averages from the (a) NCEP–NCAR reanalysis and (b) RAMS analysis. Positive (negative) values indicate an increase (decrease) in upper-level divergence, corresponding to upward (downward) motion after monsoon onset. Darker (lighter) shading and solid (dashed) contours surround positive (negative) values.

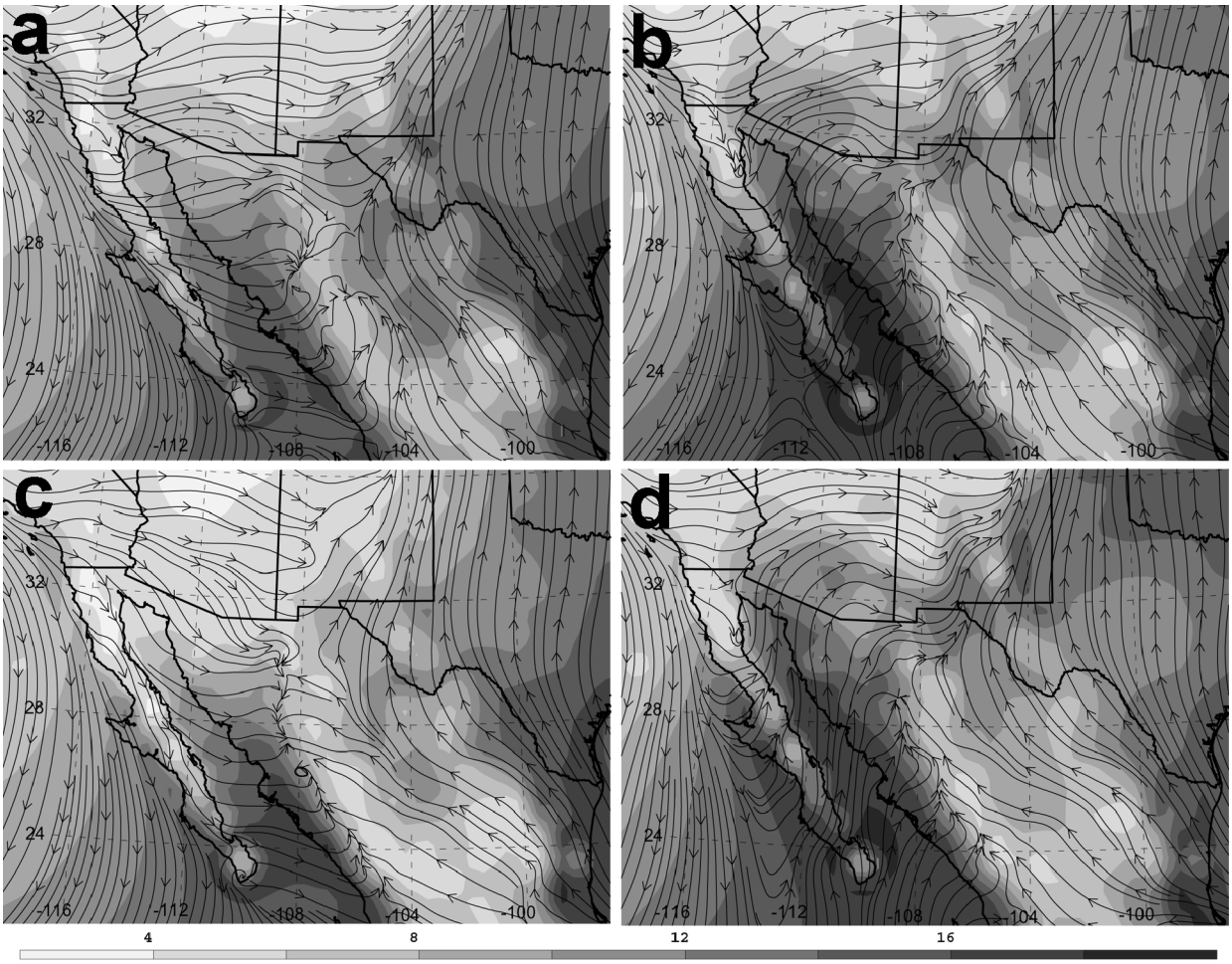

FIG. 10. Mixing ratio (shaded, g kg^{-1}) and streamlines averaged (a), (c) before and (b), (d) after onset at 233-model height. Top (bottom) panels are the 28-day (7 day) averages.

only a modest increase from ~3 to 6 (10^{-1} g kg^{-1} m s^{-1}) near the northern GoC, whereas the individual onset surge provides a significant average jump from ~3 to 11 (10^{-1} g kg^{-1} m s^{-1}). Both averaged time periods also reveal a slight weakening of the transport along the Pacific coast of Baja California. During a surge, though, the flow of air from the Pacific is still in place and it dries out as it travels over the deserts of southern California and Nevada before entering northern Arizona and New Mexico (see Fig. 10). The intrusion of this low-level dry air and strong westerly flow acts as a restrictive mechanism for the northward transport of GoC moisture; it guides the moist surge eastward and prevents the low-level moisture from advecting farther north into the central Rockies. The peak in the surge is followed by a surge retreat in the model as the large-scale flow returns toward its presurge position; at this time the enhanced moisture in Arizona and New Mexico returns to a base state with the intrusion of drier air back into Arizona.

While the GoC surge occurs, there is also an increase in the low-level transport from the GoM with the greatest increase in transport and mixing ratio contained in southern Texas and the neighboring regions of coastal Mexico. The winds from the GoM develop a more easterly component after the start of the surge. Despite a stronger easterly push of moisture from the GoM, the interior of Mexico remains relatively dry and limits the role of the GoM as a contributor of moisture to Arizona and west New Mexico at the low levels. Schmitz and Mullen (1996) and Higgins et al. (1997) also found the moisture flux from the GoM to be of little consequence in providing moisture to the Southwest at low levels, though the relative contributions of the two moisture sources was more ambiguous at the mid levels. Interacting low-level flows from the GoM and the GoC meet in western Mexico and produce a distinct convergence zone that persists along or just east of the Sierra Madres. Bryson and Hare (1974) and Adang and Gall (1989) both depict this convergence zone as the southern extension of their ''monsoon boundary'' that separates moist air from the east from the typically dry air to the

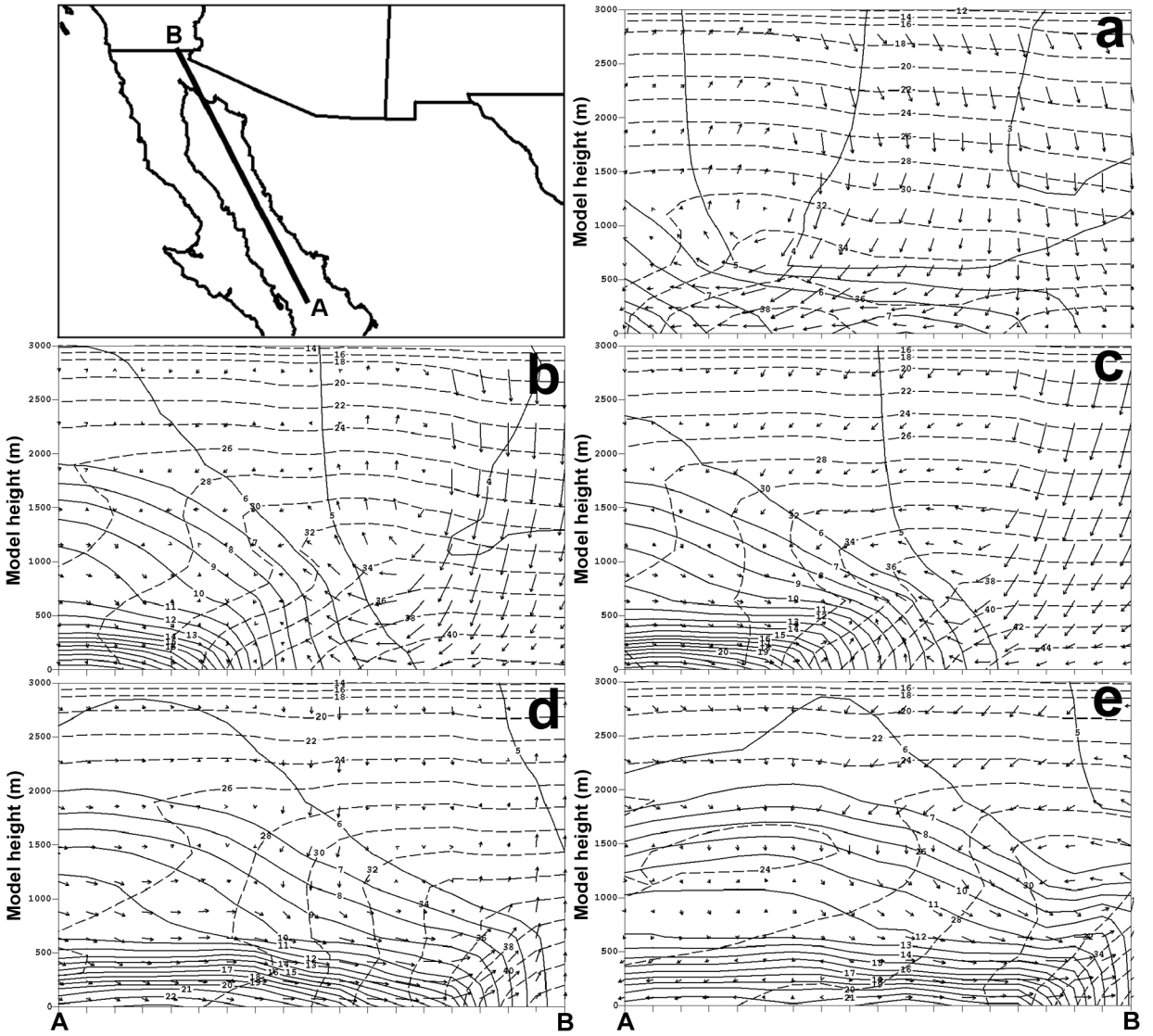

FIG. 11. Vertical cross section of model mixing ratio (g kg^{-1}, solid contours), temperature (°C, dashed contours), and circulation vectors (arrows) along the extent of the GoC from points A to B at 0000 UTC on (a) 29 Jul, (b) 31 Jul, (c) 2 Aug, (d) 4 Aug, and (e) 6 Aug 1993. This is the onset surge for the 1993 season. Tick marks are every 40-km along the length of the cross section.

west. Hales (1972) and Reyes and Cadet (1988) also conclude that the Sierra Madres pose as a large barrier to moist low-level flow from the GoM, and that the GoC is the primary source for enhanced moisture in the Southwest. From comparisons of this simulated surge event with others, this convergence zone tends to shift slightly east following a surge onset as the south-southwesterly flow from the GoC increases in strength as an onshore flow into the high terrain of western Mexico. This zone prevents the GoM flow from reaching the windward slopes of the Sierra Madres and GoC at low levels. As numerous surge events are examined in the model analyses, it is becoming more convincing that the GoM plays only a minor role in the contribution of low-level moisture to the desert Southwest. The warm waters of the GoC and the elevated convection along the SMO are the greatest contributors of moisture and precipitation to Arizona and western New Mexico within these simulations.

The Great Plains LLJ is known as a significant moisture transport mechanism for convection and precipitation generation over the plains and points downstream during the late spring and summer months. Such precipitation development hinges upon a very moist near-surface layer provided by the LLJ and lifting provided by the ageostrophic circulations associated with the jet (Uccellini and Johnson 1979). Following monsoon onset, the model-simulated Great Plains LLJ over east Texas, on average, weakens with the westward shift in the 500-mb anticyclone. The 28-day averages in the mois-

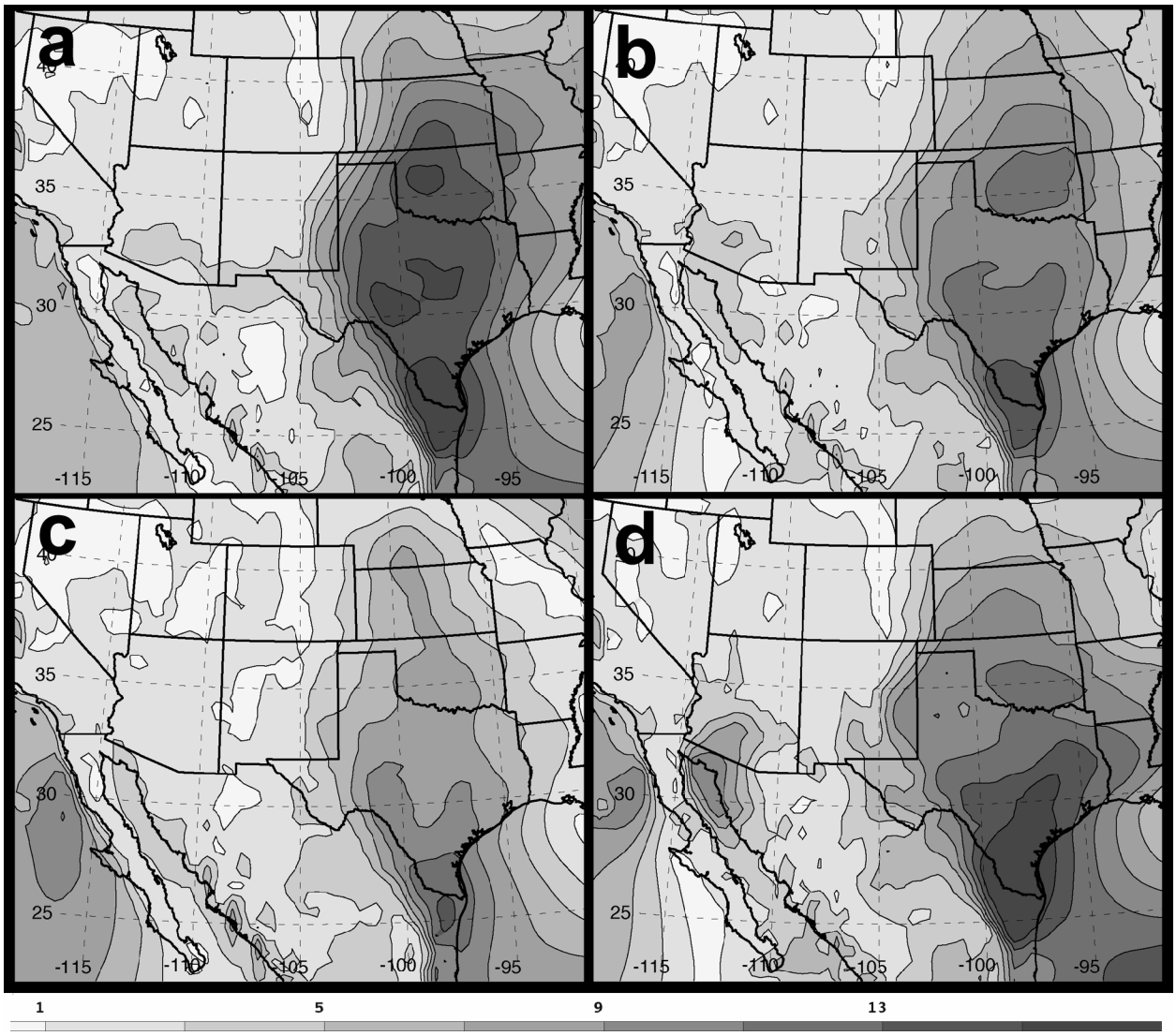

FIG. 12. Moisture transport (10^{-1} g kg^{-1} m s^{-1}) averaged (a), (c) before and (b), (d) after onset at 233-m model height. Top (bottom) panels are the 28-day (7 day) averages.

ture transport from Fig. 12 reveal a reduction in the flux of moisture from the GoM following onset, while the 7-day average reveals a slight increase, with the greatest change occurring along the southernmost coastal region of Texas near the Mexican border. The strength of the Great Plains moisture transport varies between surge events as the large-scale flow experiences periods of oscillation, but the seasonal average favors a weakening of this transport.

Figures 13a and 13b reveal the average ''decrease'' in moisture transport at 233 and 2280 m above the surface; the near-surface level shows a decrease from the western GoM through Texas, the central plains, and into the Midwest. In contrast, there is relatively little decrease in the transport at 2280 m except in Illinois and eastern Missouri. Without the low-level moisture and transport mechanism, the likelihood of self-generated convection and widespread precipitation is diminished over this region following onset. Studies of precipitation production over the central plains have shown that a large portion of the rain that falls over the Great Plains from late spring through the summer comes from mesoscale convective systems (MCS) (e.g., Maddox 1980; Fritsch et al. 1986; Jirak et al. 2003). Monthly averages of GOES satellite-derived cloud top temperature reveal a definitive shift in the primary locations of MCSs in the United States throughout the summer (Douglas et al. 1993). From June to July the zone of coldest cloud tops transits from the central plains to the northern plains and northern tier region, with activity extending north and east from the eastern plains of Colorado. This shift in the location of convective activity agrees with the similar shift of the time-averaged vertical velocity and precipitation fields (from Fig. 8).

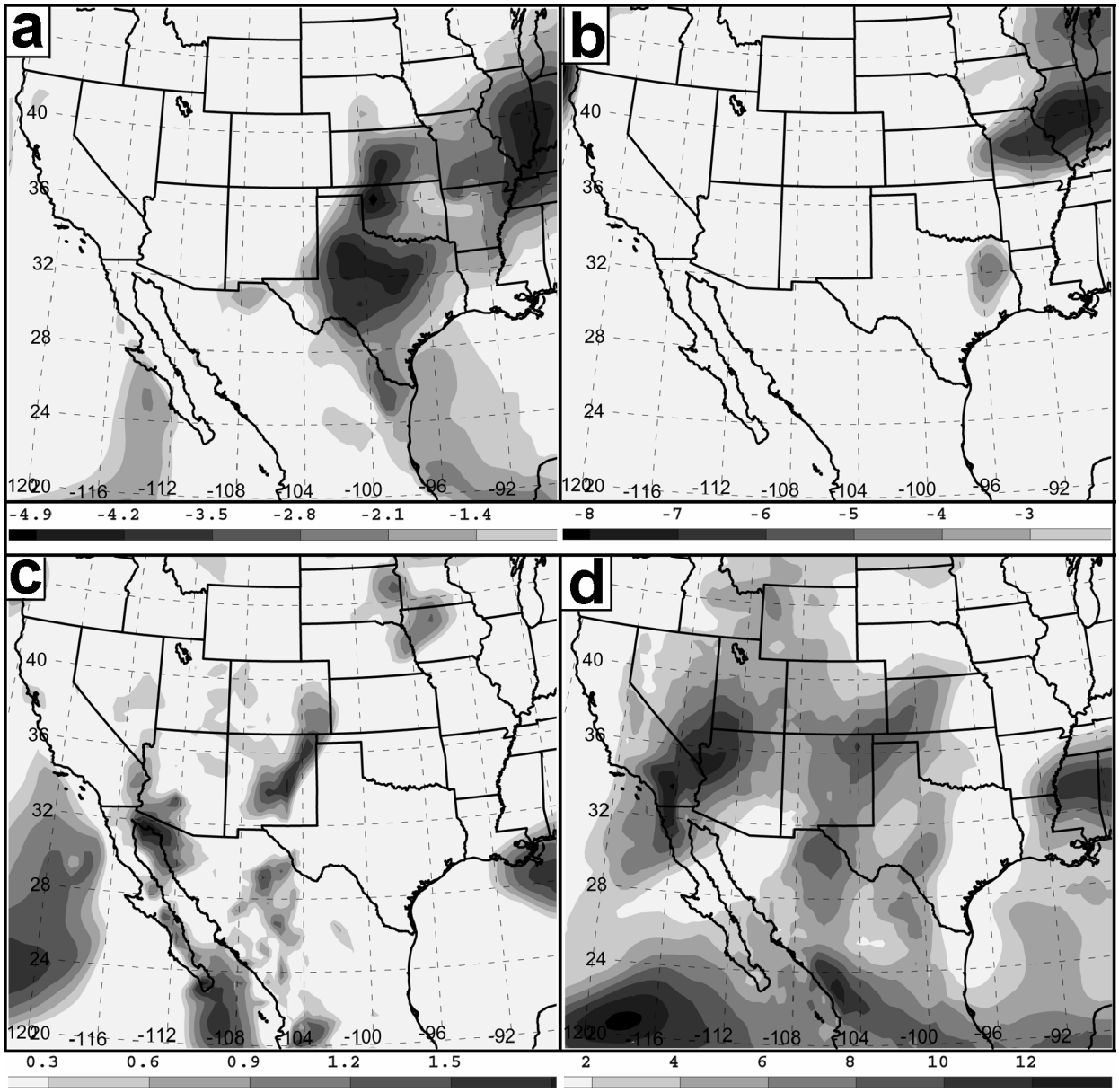

FIG. 13. Average moisture transport (10^{-1} g kg^{-1} m s^{-1}) (top) decrease and (bottom) increase following monsoon onset at model heights of (a), (c) 233 and (b), (d) 2280 m. Values indicate the subtraction of the 28-day preonset average from the postonset average.

From the opposite perspective, the average ''increase'' in moisture transport (Figs. 13c and 13d) reveals enhanced low-level transport along the extent of the GoC, New Mexico, southeast Colorado, the Sierra Madres, and over the Pacific offshore of Baja. At the 2280-m level the strengthening of the moisture flux is increased substantially over a broad region covering much of Mexico, New Mexico, west Texas, and from the Pacific near southern California into western Arizona. The coastal Pacific is typically less emphasized as a significant moisture source when compared to the GoM and GoC, but these model analyses and those of Douglas et al. (1993) and Cavazos et al. (2002) suggest the Pacific to be a contributing source of moisture for precipitation in the Southwest. Much of the transport increase from the GoM enters south of the Texas–Mexico border and is transported northwestward toward central Mexico and up into central and eastern New Mexico. This flux of moisture remains along and toward the eastern side of the typical location of the monsoon boundary. The location of this increase in moisture flux mimics the pattern of increased precipitation, and it is positioned along the west–east gradient region of the seasonal-accumulated precipitation pattern in eastern New Mexico and Colorado. Others have also suggested that GoM moisture at mid levels may contribute to monsoonal precip-

itation in Mexico, Arizona, and New Mexico (e.g., Reyes and Cadet 1988; Adang and Gall 1989). There is also a distinct ''hole'' in the positive moisture transport field at 2280 m over northwest Mexico and southern Arizona. This north–south oriented minimum in the moisture transport field is located between two very different air masses at this level with moist, cooler air advecting from the Pacific and drier, warmer air whose original moisture source was the GoM.

Despite the limit in the northward push of low-level moisture into Arizona there is still ample moisture entering the Rocky Mountain region that is not tied directly to the GoC surge. The increase in moisture at low levels in southern Arizona aids in developing moist convection, with a concentration of systems forming along the moisture boundary between central and northern Arizona. The convection is associated with the overall increase in the vertical transport in the region, such that moisture from low levels is vertically advected to the mid- and upper levels. A cross section of the postonset average mixing ratio increase, which extends from points **A** to **B** in Fig. 14a, is shown in Figs. 14b and 14c. This figure reveals the local vertical extent of moisture and the limitation in the northern progression of monsoon-related moisture. The highest mixing ratio air is contained within 400 m of the surface, and the moist air within 1000 m of the surface is largely contained south of central Arizona and New Mexico. This plot also reveals the displacement of moisture from low to mid levels following monsoon onset; above 1000 m the excess moisture is often transported into Utah and Colorado and perhaps farther northward depending upon the strength of the monsoon. In their study of the vertical structure of the monsoon boundary, Adang and Gall (1989) also note the sharp contrast in moisture across the boundary with relatively drier air positioned to the north and west. Though the increase in moisture at mid levels is weaker than at low levels, it still represents a midlevel moisture addition to points north of central Arizona. The low- and midlevel moisture intrusions enhance the likelihood of the generation of moist convection over the typically dry Southwest. Over the high peaks and Front Range of Colorado, the combination of moist convective instability, elevated diabatic heating, ample lifting from westerly flow over the mountains, and/or lifting due to easterly upslope flow from the mountain–plains solenoid circulation tends to favor the development of the convective systems that are often observed during late afternoon during periods of increased monsoonal flow (e.g., Cotton et al. 1983; Tripoli and Cotton 1989; Nachamkin and Cotton 1998).

To further examine the relative impacts of the low- and midlevel moisture source, Fig. 15 displays the average mixing ratio difference fields for levels at 72-m, 2280-m, and 5598-m model height. Over the northern GoC an increase in mixing ratio is present at each level shown, with the maximum occurring at the lowest level. The greatest intrusion of moisture into the mountain

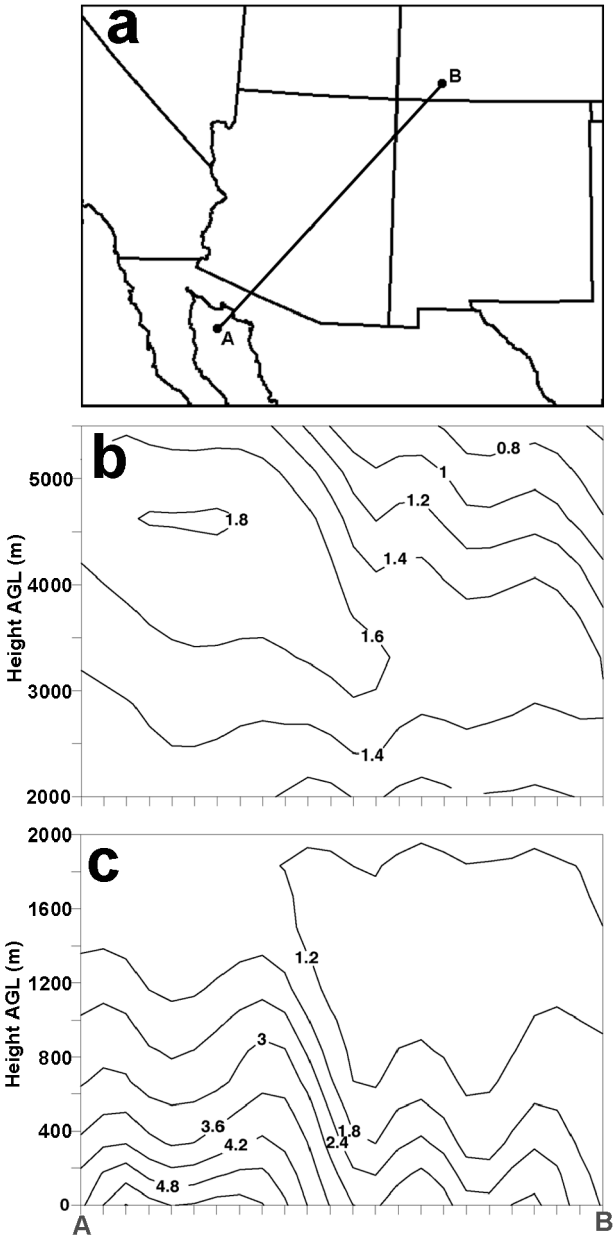

FIG. 14. Vertical cross section of the mixing ratio difference (g kg^{-1}) between the 28-day pre- and postonset averages for the transect region **A**–**B** in (a) at the model heights of (b) 2000–5000 and (c) 0–2000 m. Positive values indicate an increase in mixing ratio after monsoon onset. Note the height scale difference between panels. Tick marks are every 40 km along the length of the cross section.

west, however, occurs at the mid levels. The eastern boundary of the low-level maximum is largely collocated with the monsoon boundary. The mid- and upper-level moisture is not as bound by this dependence, and it is able to advect into Colorado and Utah. Increases in moisture well above the surface are influenced by both transport from the Pacific (see Fig. 13d) and moisture transported vertically by convection developing

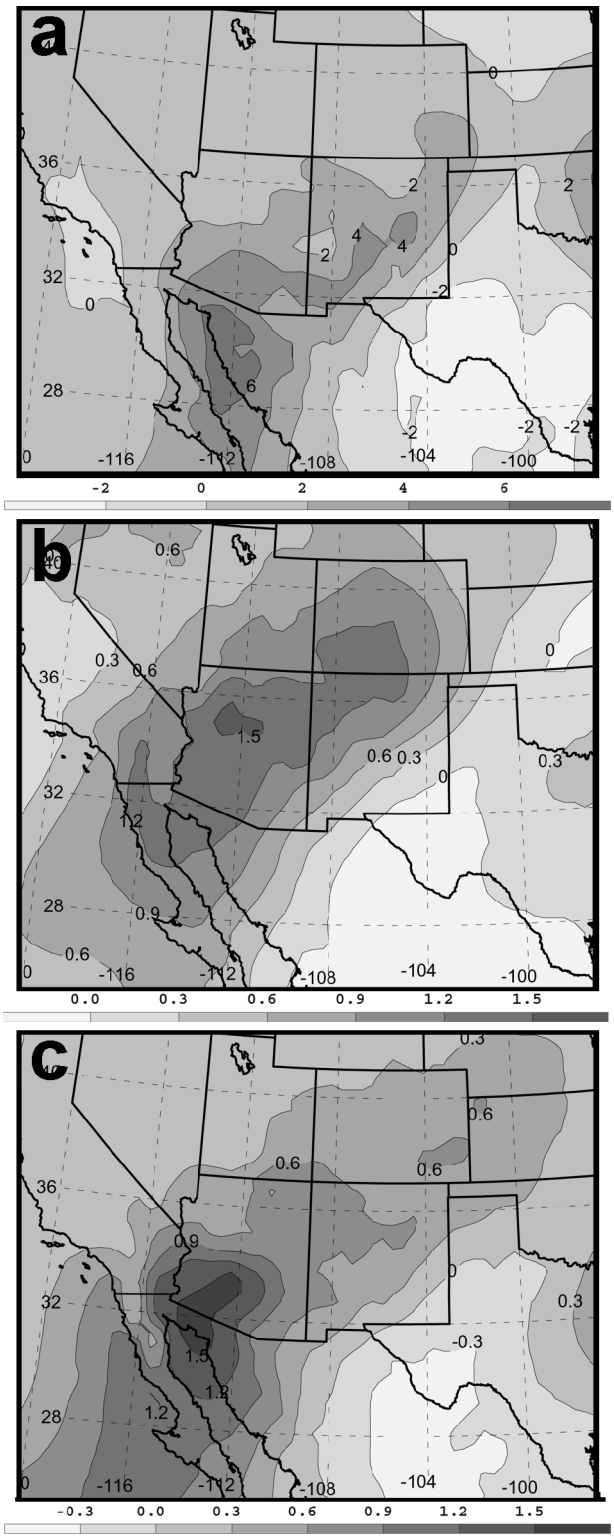

FIG. 15. Mixing ratio difference (g kg^{-1}) between the 28-day pre- and postonset averages for the following model levels: (a) 72 m, (b) 2280 m, and (c) 5598 m. Positive values indicate increases in mixing ratio following monsoon onset.

along the monsoon boundary in Arizona and New Mexico.

d. Diurnal cycle of the GoC LLJ

It is well known that one of the driving forces for the surge of the monsoon into the United States is the development of the GoC LLJ (e.g., Tang and Reiter 1984; Brenner 1974; Carleton 1986; Carleton et al. 1990; Douglas 1995). Following onset there is a change in direction from northwesterly off the Pacific to almost southerly from the GoC. This jet, along with the daily convection and precipitation, follows a diurnal cycle throughout the monsoon season that is most pronounced during surge events (Douglas 1995). The RAMS model performs well in capturing these features, as is evident from 7-day averages of the low-level winds (233 m) at 0000, 0600, 1200, and 1800 UTC following the onset surge event (Figs. 16a–d).

The development of the relatively strong low-level southerly flow from the GoC into Arizona occurs from the start of each surge event through the retreat phase. Between surge events there are periods of a day or two where the winds are more westerly, but they remain in sharp contrast to the strong northwesterly flow that persists from the Pacific prior to monsoon onset. During the monsoon surge periods there are daily fluctuations in the strength and location of the LLJ in the northern GoC. The model produces a LLJ whose strongest winds are near 233-m model height (though this peak height can vary somewhat). On average, the jet is weakest at 1800 UTC and strongest at 0600 UTC, and the jet maximum is located in the central to western part of the gulf, though the position can fluctuate between surge events. This model prediction of the LLJ varies slightly from the pilot balloon, raob, and aircraft observations of Douglas (1995), in which the jet reaches peak intensity around 1200 UTC. [It should be noted that the LLJ maximum in the model occurs on average at 0600 UTC over the northern GoC while the maximum at 1200 UTC, identified by Douglas (1995), comes largely from observations at Yuma, nearly 120 km inland. This may partially account for our disagreement in timing.] RAMS does well to predict the relative position of the jet toward the central and western portions of the GoC with maximum speed located between 250 and 400 m AGL in the northern GoC, as was noted from the aircraft observations.

An analysis of the 7-day average diurnal variability of the low-level vorticity field after onset reveals a local maximum of cyclonic vorticity along the northeast coast of Baja that is associated with the curvature in the flow as it transits from northwesterly over the Pacific to southerly over eastern Baja (Figs. 16e–h). There is also a local maximum of anticyclonic vorticity along the northwest coast of Mexico in association with the low- to midlevel anticyclone. These vorticity patterns are generally consistent with those of Douglas (1995),

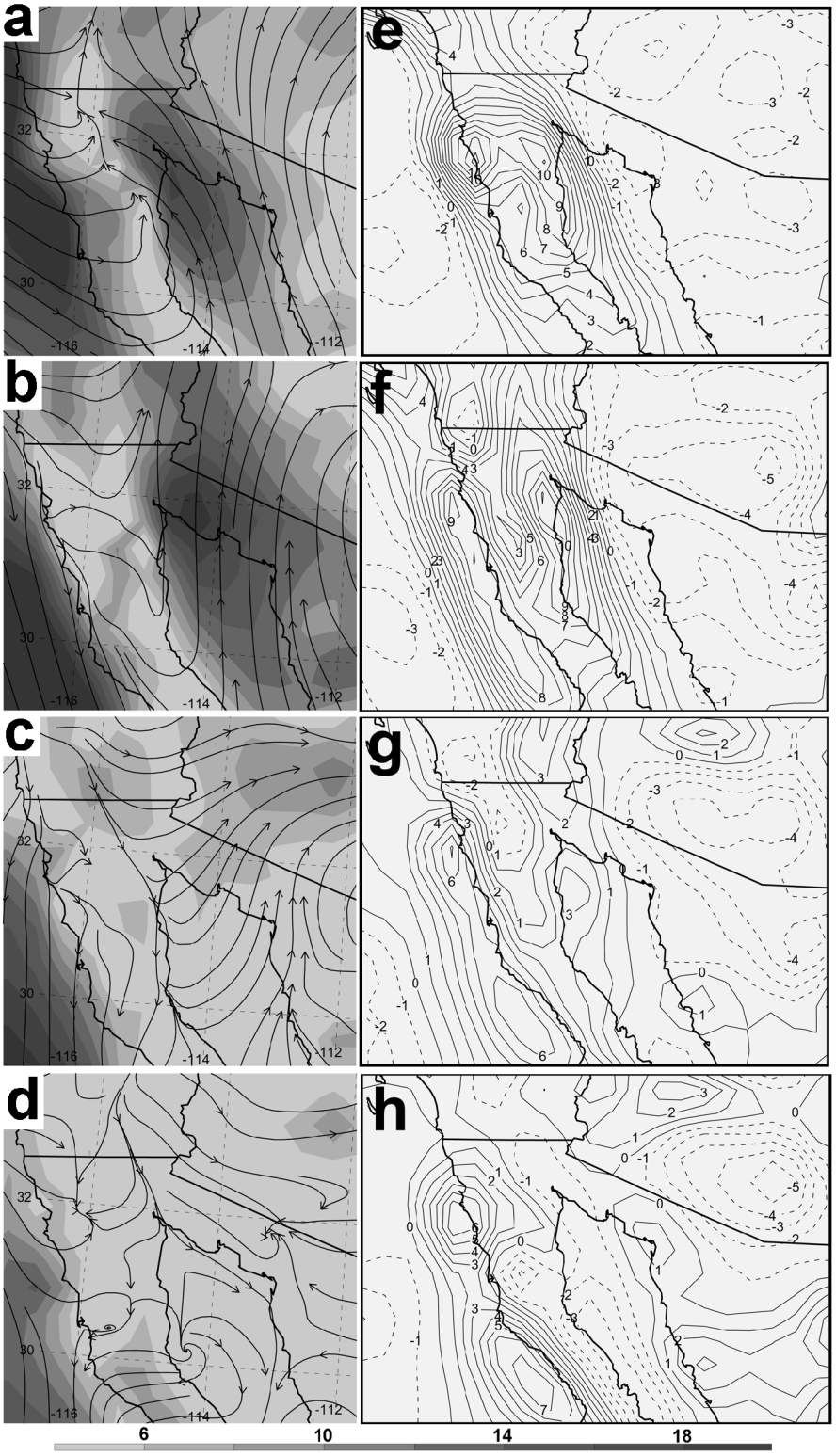

FIG. 16. Isotachs (shaded, kt) and (a)–(d) streamlines and (e)–(h) relative vorticity (s^{-1} 10^5) at 233-m model height for the 7-day averaged period after monsoon onset for the following times: (a), (e) 0000, (b), (f) 0600, (c), (g) 1200, and (d), (h) 1800 UTC. For example, (a) is the average of the 0000 UTC wind for the 7 days following the onset date.

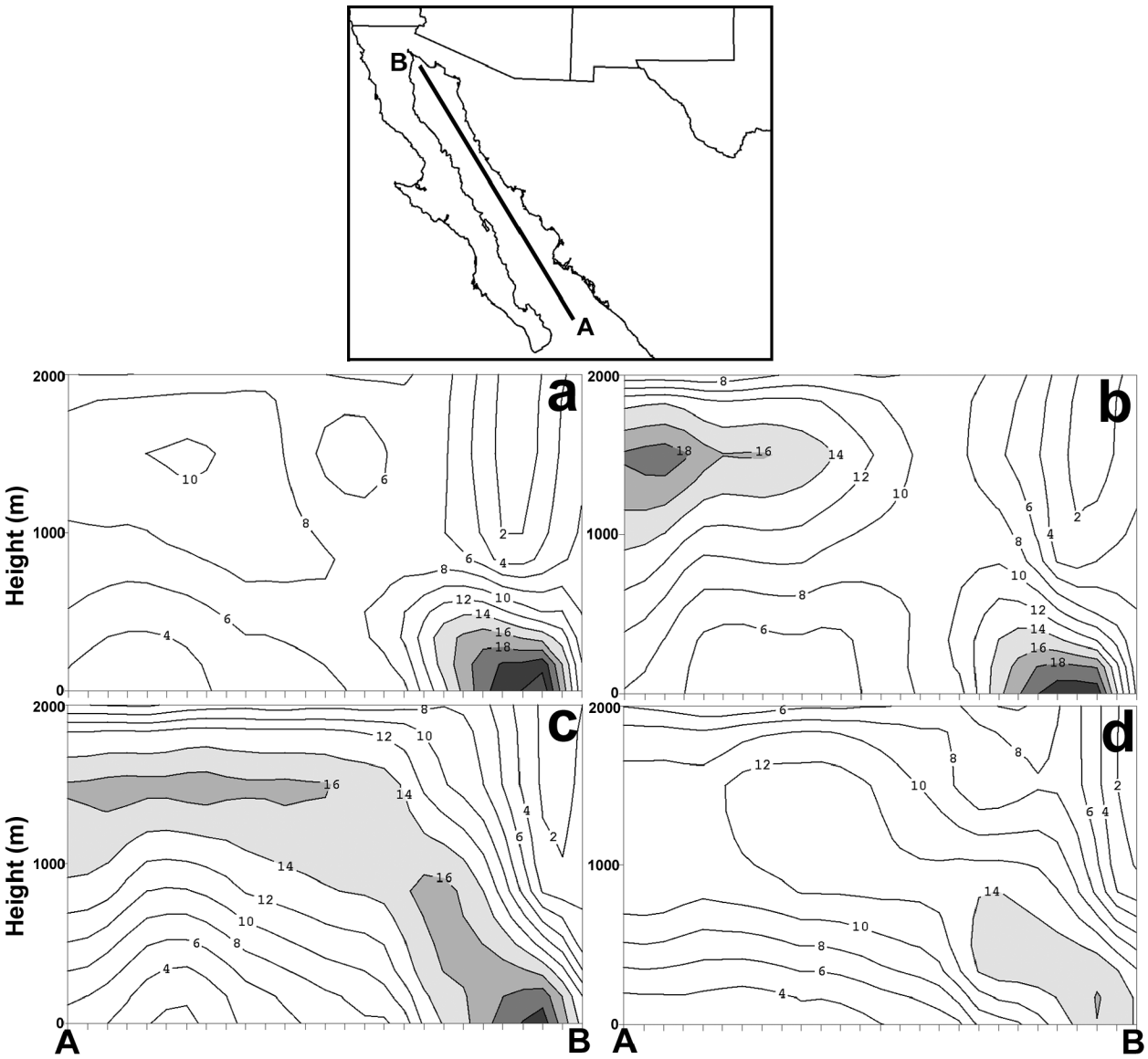

FIG. 17. Vertical cross section of model tangential winds (kt) along the length of the GoC from points **A** to **B** during the first surge on 4 Aug 1993 at (a) 0000, (b) 0600, (c) 1200, and (d) 1800 UTC. Positive values indicate southeasterly flow along the cross-sectional line. Values greater than 14 kt are shaded. Tick marks are every 40 km along the length of the cross section.

though his emphasis was in the layer from 850 to 700 mb. The simulated position and strength of the LLJ is directly linked with the location and strength of the vorticity features.

The portion of the GoC LLJ discussed thus far is known as the strongest and northernmost extent of a southerly jet that extends the length of the GoC following monsoon onset (Douglas 1995). As monsoon onset progresses northward along the west coast of Mexico, and ultimately into the United States, the jet extends its northward range of influence. Figure 17 reveals a vertical cross section of the diurnally varying tangential wind along a line that extends down the center of the gulf from its northernmost end to the tip of Baja; the tangential winds are plotted at 0000, 0600, 1200, and 1800 UTC for 4 August 1993, which is near the beginning of the first surge of 1993. One can see the very low-level nature of the jet maximum to the north, whose greatest magnitude and strongest wind speed gradient occur near 0000 or 0600 UTC; the specific time can vary daily. To the south, a second jet maximum begins to noticeably appear around 1500-m model height by 0600 UTC. By 1200 UTC it has extended northward while descending toward the surface; it has connected with the weakening near-surface jet maximum at the northern end of the GoC and has developed into a single entity from north to south with locally strong winds along the full extent. Both portions of the jet are rela-

tively weak at 1800 UTC on most days during surge events. It should be noted that the elevated wind maximum to the south of the cross section is located above the moisture surge layer, as seen in Fig. 11, and the strongest near-surface winds are near the leading edge of the moisture surge. This elevated southern wind maximum is also seen from aircraft data in Stensrud et al. (1997, their Fig. 4). Their figure reveals a local wind maximum generally located above the region of maximum moisture gradient toward the southern end of the cross section and nearly collocated wind and moisture maxima near the surface at the northern end of the cross section.

The maximum in the LLJ in the northern GoC is influenced by several factors local to the region. Seabreeze circulations along the west, north, and east coasts at the northernmost end of the GoC direct the southerly flow onshore, thereby partly contributing to the vorticity couplets on opposite sides of the GoC. The local heat low typically located near the border between California and Arizona is also known to draw in air from near the northern GoC and induce convergent flow at the surface near its center (Douglas and Li 1996). Each of these onshore flows show strengthening as the adjacent land heats up throughout the day. In addition, there is typically strong, cyclonically curved flow onshore over west Baja as the northwesterly flow from the Pacific interacts with the sea-breeze circulation and the surface friction along the terrain of northern Baja. When the flow rides over Baja and encounters the GoC on the downslope side, it is further turned cyclonically by the southerly flow and the onshore sea breeze along Baja's east coast. A strong vorticity maximum develops along the northeast coast of Baja during the heating of the day when the sea breeze is maximized. This is the time when the near-surface, northernmost LLJ begins to form and strengthen. As the evening progresses, the mesoscale circulations weaken, as does the vorticity couplet on opposite coasts of the gulf.

The southern portion of the jet tends to follow the typical diurnal cycle of a nocturnal jet with development occurring around 0600 UTC and maximum strength being reached around sunrise or near 1200 UTC for that region. In the southern GoC the Sierra Madres are much closer to the west coast of Mexico, which helps to induce more intense sea-breeze and mountain–valley-type circulations, as well as a prominent zone of baroclinicity that runs parallel to the coast. The elevated heating and mountain–sea circulation over east Baja are less intense in the model analyses than that along western Mexico, and the baroclinicity along the east coast of Baja is quite weak. The thermal wind response to the daily development of a baroclinic zone along the west coast of Mexico contributes to the southerly flow up the GoC and the diurnal oscillation that occurs.

e. Diurnal cycle of convection and precipitation

The diurnal cycle of the LLJ is accompanied by a daily cycle in the development of convection and precipitation over the SMO and U.S. Southwest. Figure 18 reveals the average precipitation rate before and after monsoon onset for model times at 0000, 0600, 1200, and 1800 UTC. For each given time of day the precipitation rate was averaged at that individual time for the 28 days before and after onset. Over the SMO and areas near the northern GoC the precipitation rate is at its

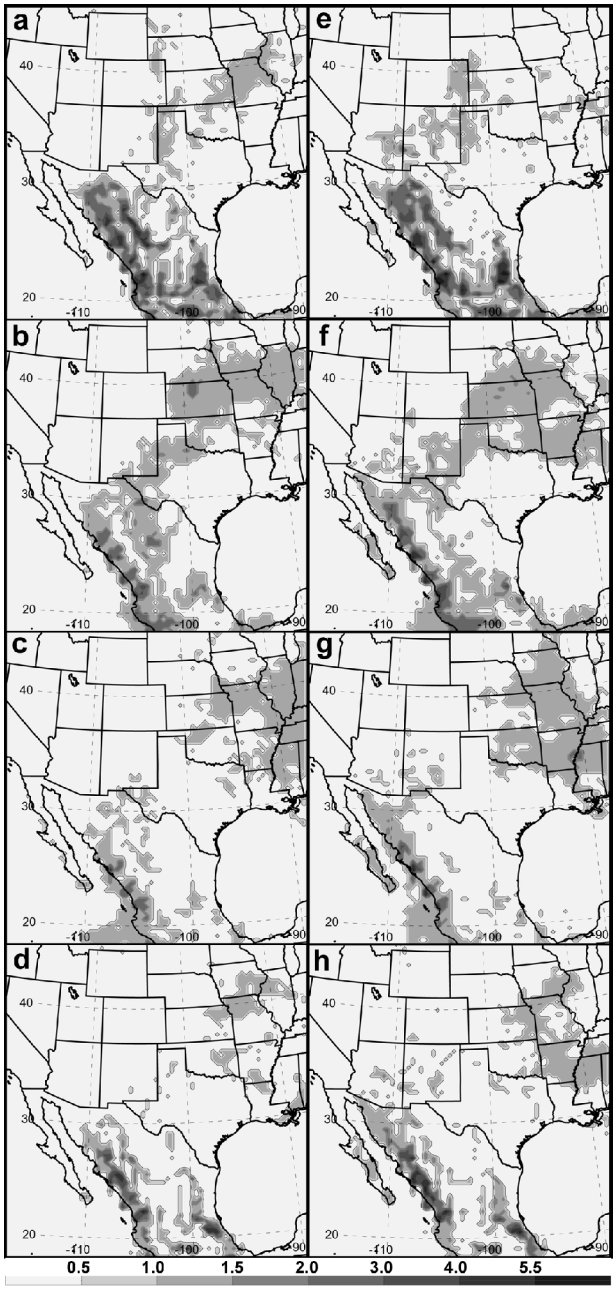

FIG. 18. Model precipitation rate (10^2 h^{-1}) averaged (a)–(d) before and (e)–(h) after monsoon onset for the following times of day: (a), (e) 0000, (b), (f) 0600, (c), (g) 1200, and (d), (h) 1800 UTC. Fields are averaged for the 28-day period pre- and postmonsoon onset. For example, (a) is the average of the 0000 UTC precipitation rate for the 28 days prior to onset.

greatest extent near 0000 UTC; this is also true for the development of systems near the Front Range of the Rocky Mountains. The maximum over the central plains tends to occur near 0600 UTC, and over the Midwest and lower Mississippi valley around 1200 UTC. Generally, before and after the start of the monsoon, the extent of precipitation is at a minimum at 1800 UTC over the United States and at 1200 UTC along the SMO. These model-derived, diurnally varying precipitation patterns agree with the typical summertime precipitation over the United States and Mexico. Convection forms in the late afternoon (0000 UTC), propagates onto the plains by late evening (0600 UTC), and to the Midwest by morning (1200 UTC) (Wallace 1975; Carbone et al. 2002).

There are several observations to highlight concerning the significant increase in the diurnal variability of precipitation between the periods prior to and following the onset of the monsoon (e.g., Wallace 1975). Among the four averaged times of day, the greatest broad-scale change in the extent of precipitation following the onset date is evident at 0000 UTC. At this time there is a marked increase in precipitation rate over Arizona, New Mexico, and Colorado, and there is also a considerable decrease over the eastern plains and Midwest (Nebraska, Missouri, and Illinois). At 0600 UTC the most noticeable differences are the increase in precipitation over Arizona, New Mexico, and the Arkansas region and a decrease over portions of the upper Midwest. Over Mexico the precipitation increases along the SMO and extreme northwest Mexico near the GoC. The broad region of precipitation to the east of the Sierra Madres that is present before onset becomes much less evident following onset. At both 1200 and 1800 UTC, Arizona, New Mexico, Arkansas, the Midwest, and extreme northwest Mexico all show increases in the average precipitation after onset; differences over the SMO are rather minimal for these times. In agreement with Higgins et al. (1998), the nighttime precipitation (0000 and 0600 UTC) generally exceeds daytime precipitation over the Southwest and Great Plains during the summer months with this observation being further enhanced following onset. Only minor changes in the precipitation over the core monsoon region between the averaged time periods are evident because the chosen onset date corresponds to the start of the monsoon in the United States; the monsoon is evident over central and south Mexico for weeks prior to the 3 August start date.

When comparing the diurnal cycles of precipitation and the LLJ there is approximately a 6-h lag between the time of maximum intensity of the LLJ and the time of maximum precipitation over the extreme northwest corner of Mexico and the southern border of Arizona. The GoC LLJ begins its daily building phase by 0000 UTC; at this time the precipitation rate along the SMO is at its daily maximum, while very little to no precipitation is evident north of the LLJ. The southern extension of the LLJ has little influence on the terrain-induced convection along the SMO except to provide an onshore sea-breeze component to the flow. Convective precipitation near the northern border of the GoC is more influenced by the moisture convergence near the terminus of the LLJ and the direct sea-breeze circulation. By 0600 UTC the precipitation rate increases in extreme northwest Mexico and the southernmost portions of Arizona in response to the increased strength and onshore propagation of the GoC LLJ. At 1200 and 1800 UTC the convection and precipitation over this region remains above the daily minimum during the weakening phase of the LLJ. Between 1800 and 0000 UTC the precipitation finally diminishes following the demise of the LLJ and the return of northwesterly flow over the northern GoC and southern Arizona. This cycle continues to repeat during surge episodes.

f. Accumulated precipitation

Much of the monsoon seasonal precipitation in both Mexico and the United States is convectively generated, and thus the model relies upon the ability of the convection parameterizations for the most accurate quantitative precipitation forecast. Until recently, the Kuo convection scheme was the only one available in the supported version of RAMS; this scheme tends to underpredict precipitation over the plains of the United States and overpredict precipitation over areas of steep topography, primarily along the monsoon region of the SMO. The Kain–Fritsch scheme was recently interfaced with RAMS and the convection trigger function was adjusted in the model to better represent the observed precipitation over the SMO (Castro et al. 2002).

Figure 19 displays the observed and model-accumulated precipitation from 4 July to 31 August 1993 for the monsoon source region and the United States. Both Kuo and Kain–Fritsch schemes perform better depending upon the location. Within the core monsoon region, along the windward and lee slopes of the Sierra Madres, the simulations using the Kain–Fritsch scheme reduce the overestimation in total rainfall and areal coverage that is produced by the Kuo scheme along this region of steep topography. The simulation with the Kuo scheme overpredicts orographic convection and the associated seasonal precipitation over the SMO. Both simulations tend to produce localized precipitation maxima that correlate with the steepest and highest topography, though the adjustment of the convection trigger function in the Kain–Fritsch scheme reduces these precipitation features in the model. Gochis et al. (2002) also performed a model intercomparison study with several cumulus parameterization schemes and found the Kain–Fritsch to outperform the others in terms of the moisture distribution and surface precipitation.

Due to a lack of rain gauge data in some remote portions of Mexico along the northern and southern extent of the Sierra Madres, we cannot verify to what extent the model-simulated orographic rainfall is ac-

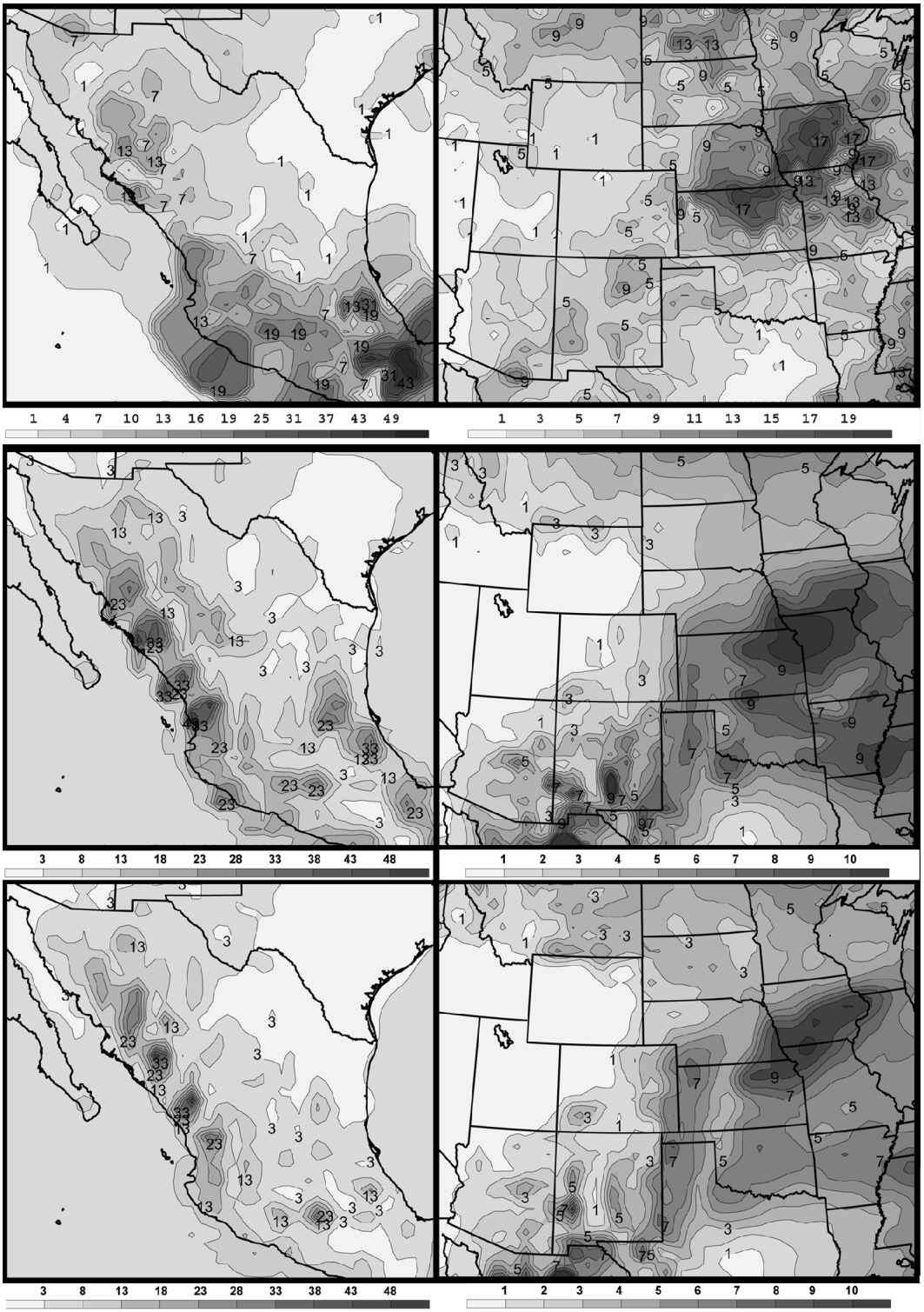

FIG. 19. Accumulated precipitation (in.) from (top) observations and RAMS simulations using the (middle) Kuo or (bottom) Kain–Fritsch convection parameterization for the period from 4 Jul to 31 Aug 1993. Observational data are plotted from daily rain gauge data in the United States and Mexico for the declustered stations shown in Fig. 4. Values over ocean areas in the observational plots are a result of objectively interpolating the gauge data to the RAMS grid. Note that the contour and shading scales vary among panels.

curate. As seen from the Mexico rain gauge network (Fig. 4), there are significant gaps in station positioning over some of the most mountainous terrain. Over southeast Mexico, along the GoM, there are also distinct differences in total rainfall produced between the simulations with different convection schemes. The observational data indicates that this region of Mexico receives the greatest amount of rainfall for the duration of the simulated time period, in excess of 43 in. in nearly 2 months time. Both simulations underestimate the total precipitation, though the model run with the Kuo scheme performs the best and produces ample precipitation, while the Kain–Fritsch scheme simulates very little rainfall in all of southeast Mexico. The regional maximum for the Kuo scheme reaches 33 in., while Kain–Fritsch only produces a very local small maximum of 13 in. Neither scheme performs best over all of Mexico during the monsoon period.

In terms of reproducing the observational data, the RAMS simulations perform relatively better over the United States than over Mexico, though, the verifying rain gauge network is more temporally and spatially continuous over the United States as well. Neither convection scheme is spectacular in simulating precipitation amounts, but both capture rainfall patterns of regional maxima quite well. The mountainous regions of the western United States do not appear to have the same influence on the convection scheme as is present along the slopes of western Mexico. Typically, though, convection does not tend to be as widespread over the Rocky Mountains compared to the SMO, and there is considerably less moisture and CAPE available for convective precipitation over the Rocky Mountains. The largest discrepancy between the model and the observed precipitation appears over the Midwest and central plains, which were inundated with flooding rains prior to the 3 August monsoon onset. Simulations running both Kuo and Kain–Fritsch schemes adequately resolve the location and precipitation pattern over the Midwest, but they tend to underestimate the precipitation maximum over this region by nearly one-half. From the plots of both observed and simulated U.S. rainfall, the most noticeable feature is the maximum observed rainfall extending from north-central Kansas to northeast Iowa. While both convection schemes produce nearly the same rainfall maximum, the locations vary slightly. The Kuo scheme tends to shift this quasi-linear rainfall pattern toward the south into north-central Missouri, whereas the Kain–Fritsch simulation produces a precipitation field in the correct location in central Iowa.

Gochis et al. (2002) also emphasized the differing circulation patterns that result with use of different cumulus parameterizations. They ultimately found that simulations with the Kain–Fritsch scheme produced broader-scale low-level convergence over Mexico and the U.S. Southwest and a more southerly component of the low-level flow over the GoC when compared against simulations using the Grell and Betts–Miller–Janjić schemes. [See Gochis et al. (2002) for references to these schemes.] When comparing the RAMS simulations using the Kuo and Kain–Fritsch schemes, the simulations with Kain–Fritsch tended to produce broader-scale near-surface convergence, while the simulations with Kuo resulted in more isolated features, especially in regions of significant topography. From examining the low-level flow over the GoC, the Kuo simulation produced the more southerly component to the flow, while the resulting circulation from the Kain–Fritsch simulation tended to be more onshore along the central and southern coasts of west Mexico. Over the northern GoC, in the vicinity of the strongest winds from the LLJ, the flows were very similar to the Kain–Fritsch simulation, producing a slightly weaker LLJ in magnitude and expanse. Further comparisons of these parameterizations in the future will help shed light on their applicability and skill in regional climate simulations using the RAMS mesoscale model.

4. Summary

Seasonal simulations of the North American monsoon by the RAMS model perform quite well in resolving and reproducing the large- and mesoscale flow regimes, including the positioning of the U.S. high pressure ridge, which largely controls the timing and strength of the monsoon, and the diurnally varying LLJ along the GoC and western Mexico. While the imposed light internal gridpoint nudging helps prevent the model-predicted large-scale fields from deviating too far from reality over time, it does not inhibit the model in producing the mesoscale flows necessary for the development of the surge events that are the emphasis of the monsoon season. The model retains the freedom to sensitively vary with the use of different convection schemes and prescribed soil moisture and SSTs. The model does well to capture the westward displacement of the large-scale anticyclone over the central United States, the similar westward displacement in the vertical velocity and precipitation field, and the associated surges of low-level moisture from the northern GoC into the U.S. Southwest. Low- and midlevel plots of mixing ratio and moisture transport point to the GoC LLJ as the primary moisture source and advection mechanism for the formation of moist convection in the desert Southwest. The eastern Pacific and GoM act as moisture sources at the mid levels into western Arizona and eastern New Mexico, respectively. The GoM provides moisture along the eastern side of the monsoon boundary, and the transport from the Pacific extends its range of influence in Utah and Colorado over regions in which elevated convection becomes more frequent and widespread following monsoon onset.

RAMS also does well in simulating the increased magnitude of the diurnal variability of the GoC LLJ and convection over the SMO and United States following onset. There is a definitive shift toward increased night-

time precipitation over the U.S. Southwest and northwest Mexico and increased daytime precipitation over the Great Plains and Midwest. Moisture surges and the GoC LLJ display a very distinct diurnal cycle, with the LLJ at its averaged maximum at 0600 UTC near the north-central to western GoC. The 1200 UTC LLJ appears to be relatively weaker and more onshore into southern Arizona. These averaged times in the model differ from the observational study of Douglas (1995), though it should be noted that the time of the jet maximum strength varies between modeled surges; several surge days place the timing of the jet maximum at 1200 UTC.

Simulating the seasonal accumulated precipitation is a more difficult matter, considering the quasi-hemispheric domain that includes both tropical and midlatitude regions that are characterized by both flat and steep terrain. Precipitation totals tend to be overestimated along the mountainous terrain of Mexico and underestimated over the U.S. Midwest. Both Kuo and Kain–Fritsch convection parameterizations were utilized in the model, with each one outperforming the other over different regions of the domain. Kain–Fritsch better reproduces the magnitude and amount of precipitation over western Mexico, while Kuo performs better over eastern Mexico near the region influenced by the onshore flow of the GoM. Over the United States, Kain–Fritsch and Kuo produce very similar rainfall magnitudes, while Kain–Fritsch tends to provide a better spatial correlation to the observed precipitation over the 1993 flood region of the Midwest.

As other seasonal and sensitivity test simulations are examined, we will be able to provide further insight into the ability of the RAMS model to accurately simulate the monsoonal flow and determine its best capabilities and deficiencies. With the given limitations in simulating precipitation, it is possible that the model will perform better for the 1988 (drought year) and 1997 (El Niño) simulations. These further simulations will also provide a good interannual comparison for these other ''extreme'' wet and dry monsoon years that were chosen for simulation. This will give us a better handle as to which conditions are best simulated by the RAMS model and provide more information for working to improve model realizations.

Part II will focus on the interseasonal comparisons between the 1988, 1993, and 1997 monsoon seasons and sensitivity to soil moisture and SSTs. Part III of this paper will present evidence concerning the development and impacts of mid- to upper-level potential vorticity anomalies that originate from the core monsoon region and along the monsoon boundary near Colorado.

Acknowledgments. This research was supported by a grant from the National Oceanic and Atmospheric Administration under Contract NA17RJ1228. We would like to thank Dr. Art Douglas of Creighton University for graciously providing us with the daily rain gauge data from Mexico. These datasets have been most helpful for our soil moisture estimations and rainfall validation.

REFERENCES

Adang, T. C., and R. L. Gall, 1989: Structure and dynamics of the Arizona monsoon boundary. *Mon. Wea. Rev.,* **117,** 1423–1438.

Badan-Dangon, A., C. E. Dorman, M. A. Merrifield, and C. D. Winant, 1991: The lower atmosphere over the Gulf of California. *J. Geophys. Res.,* **96,** 877–896.

Blanchard, B. J., M. J. McFarland, T. J. Schmugge, and E. Rhoades, 1981: Estimation of soil moisture with API algorithms and microwave emission. *Water Resour. Bull.,* **17,** 767–774.

Brenner, I. S., 1974: A surge of maritime tropical air—Gulf of California to the southwestern United States. *Mon. Wea. Rev.,* **102,** 375–389.

Bryson, R. A., and W. P. Lowry, 1955: The synoptic climatology of the Arizona summer precipitation singularity. *Bull. Amer. Meteor. Soc.,* **36,** 329–339.

——, and F. K. Hare, 1974: The climates of North America. *Climates of North America,* World Survey of Climatology, Vol. 11, Elsevier, 1–45.

Carbone, R. E., J. D. Tuttle, D. A. Ahijevych, and S. B. Trier, 2002: Inferences of predictability associated with warm season precipitation episodes. *J. Atmos. Sci.,* **59,** 2033–2056.

Carleton, A. M., 1986: Synoptic–dynamic character of ''bursts'' and ''breaks'' in the south-west U.S. summer precipitation singularity. *J. Climatol.,* **6,** 605–623.

——, 1987: Summer circulation of the American southwest, 1945–1984. *Ann. Assoc. Amer. Geogr.,* **77,** 619–634.

——, D. A. Carpenter, and P. J. Weser, 1990: Mechanisms of interannual variability of the southwest United States summer rainfall maximum. *J. Climate,* **3,** 999–1015.

Castro, C. L., W. Y. Y. Cheng, A. B. Beltran, R. A. Pielke Sr., and W. R. Cotton, 2002: The incorporation of the Kain–Fritsch cumulus parameterization scheme in RAMS with a terrain-adjusted trigger function. *Fifth RAMS Users and Related Applications Workshop,* Santorini, Greece, ATMET, Inc.

Cavazos, T., A. C. Comrie, and D. M. Liverman, 2002: Intraseasonal variability associated with wet monsoons in southeast Arizona. *J. Climate,* **15,** 2477–2490.

Cotton, W. R., R. L. George, P. J. Wetzel, and R. L. McAnelly, 1983: A long-lived mesoscale convective complex. Part I: The mountain-generated component. *Mon. Wea. Rev.,* **111,** 1893–1918.

——, and Coauthors, 2003: RAMS 2001: Current status and future directions. *Meteor. Atmos. Phys.,* **82,** 5–29.

Douglas, M. W., 1995: The summertime low-level jet over the Gulf of California. *Mon. Wea. Rev.,* **123,** 2334–2347.

——, and S. Li, 1996: Diurnal variation of the lower-tropospheric flow over the Arizona low desert from SWAMP-1993 observations. *Mon. Wea. Rev.,* **124,** 1211–1224.

——, R. A. Maddox, K. Howard, and S. Reyes, 1993: The Mexican monsoon. *J. Climate,* **6,** 1665–1677.

Fritsch, J. M., R. J. Kain, and C. R. Chelius, 1986: The contribution of mesoscale convective weather systems to the warm-season precipitation in the United States. *J. Climate Appl. Meteor.,* **25,** 1333–1345.

Fuller, R. D., and D. J. Stensrud, 2000: The relationship between tropical easterly waves and surges over the Gulf of California during the North American monsoon. *Mon. Wea. Rev.,* **128,** 2983–2989.

Gochis, D. J., W. J. Shuttleworth, and Z. L. Yang, 2002: Sensitivity of the modeled North American monsoon regional climate to convective parameterization. *Mon. Wea. Rev.,* **130,** 1282–1298.

Hales, J. E., Jr., 1972: Surges of maritime tropical air northward over the Gulf of California. *Mon. Wea. Rev.,* **100,** 298–306.

Harrington, J. Y., 1997: The effects of radiative and microphysical processes on simulated warm and transition season Arctic stratus.

Ph.D. dissertation, Dept. of Atmospheric Science Paper No. 637, Colorado State University, Fort Collins, CO, 289 pp.

——, T. Reisin, W. R. Cotton, and S. M. Kreidenweis, 1999: Cloud resolving simulations of Arctic stratus. Part II: Transition-season clouds. *Atmos. Res.,* **55,** 45–75.

Higgins, R. W., Y. Yao, and X. Wang, 1997: Influence of the North American monsoon system on the U.S. summer precipitation regime. *J. Climate,* **10,** 2600–2622.

——, K. C. Mo, and Y. Yao, 1998: Interannual variability of the U.S. summer precipitation regime with emphasis on the southwestern monsoon. *J. Climate,* **11,** 2582–2606.

Jirak, I. L., W. R. Cotton, and R. L. McAnelly, 2003: Satellite and radar survey of mesoscale convective system development. *Mon. Wea. Rev.,* **131,** 2428–2449.

Jurwitz, L., 1953: Arizona's two-season rainfall pattern. *Weatherwise,* **6** (4), 96–99.

Kain, J. S., and J. M. Fritsch, 1990: A one-dimensional entraining/detraining plume model and its application in convective parameterization. *J. Atmos. Sci.,* **47,** 2784–2802.

——, and ——, 1992: The role of the convective ''triggering function'' in numerical forecasts of mesoscale convective systems. *Meteor. Atmos. Phys.,* **49,** 93–106.

——, and ——, 1993: Convective parameterization for mesoscale models: The Kain–Fritsch scheme. *The Representation of Cumulus Convection in Numerical Models, Meteor. Monogr.,* No. 46, Amer. Meteor. Soc., 165–170.

Klemp, J. B., and R. B. Wilhelmson, 1978: The simulation of three-dimensional convective storm dynamics. *J. Atmos. Sci.,* **35,** 1070–1096.

Kuo, H. L., 1965: On formation and intensification of tropical cyclones through latent heat release by cumulus convection. *J. Atmos. Sci.,* **22,** 40–63.

——, 1974: Further studies of the parameterization of the influence of cumulus convection on large-scale flow. *J. Atmos. Sci.,* **31,** 1232–1240.

Maddox, R. A., 1980: Mesoscale convective complexes. *Bull. Amer. Meteor. Soc.,* **61,** 1374–1387.

Mellor, G. L., and T. Yamada, 1974: A hierarchy of turbulence closure models for planetary boundary layers. *J. Atmos. Sci.,* **31,** 1791–1806.

Mo, K. C., J. N. Paegle, and R. W. Higgins, 1997: Atmospheric processes associated with summer floods and droughts in the central United States. *J. Climate,* **10,** 3028–3046.

Nachamkin, J. E., and W. R. Cotton, 1998: Interacting solenoidal circulations and their role in convective orogenesis. Preprints, *Eighth Conf. on Mountain Meteorology,* Flagstaff, AZ, Amer. Meteor. Soc., 11.4.

Reyes, S., and D. L. Cadet, 1988: The southwest branch of the North American monsoon during summer 1979. *Mon. Wea. Rev.,* **116,** 1175–1187.

Reynolds, R. W., and T. M. Smith, 1994: Improved global sea surface temperature analyses using optimum interpolation. *J. Climate,* **7,** 929–948.

Sadler, J. C., M. A. Lander, A. M. Hori, and L. K. Oda, 1987: *Pacific Ocean.* Vol. 2. *Tropical Marine Climatic Atlas,* Dept. of Meteorology Atlas UHMET 87-02, University of Hawaii, 27 pp.

Schmitz, J. T., and S. Mullen, 1996: Water vapor transport associated with the summertime North American monsoon as depicted by ECMWF analyses. *J. Climate,* **9,** 1621–1634.

Smagorinsky, J., 1963: General circulation experiments with the primitive equations. *Mon. Wea. Rev.,* **91,** 99–164.

Stensrud, D. J., R. L. Gall, S. L. Mullen, and K. W. Howard, 1995: Model climatology of the Mexican monsoon. *J. Climate,* **8,** 1775–1794.

——, ——, and M. K. Nordquist, 1997: Surges over the Gulf of California during the Mexican monson. *Mon. Wea. Rev.,* **125,** 417–437.

Tang, M., and E. R. Reiter, 1984: Plateau monsoons of the Northern Hemisphere: A comparison between North America and Tibet. *Mon. Wea. Rev.,* **112,** 617–637.

Tripoli, G. J., and W. R. Cotton, 1989: Numerical study of an observed orogenic mesoscale convective system. Part I: Simulated genesis and comparison with observations. *Mon. Wea. Rev.,* **117,** 273–304.

Uccellini, L. W., and D. R. Johnson, 1979: The coupling of upper and lower tropospheric jet streaks and implications for the development of severe convective storms. *Mon. Wea. Rev.,* **107,** 682–703.

Walko, R. L., W. R. Cotton, J. L. Harrington, and M. P. Meyers, 1995: New RAMS cloud microphysics parameterization. Part I: The single-moment scheme. *Atmos. Res.,* **38,** 29–62.

Wallace, J. M., 1975: Diurnal variations in precipitation and thunderstorm frequency over the conterminous United States. *Mon. Wea. Rev.,* **103,** 406–419.